NRC·CNRC

NRC Publications Archive
Archives des publications du CNRC

Proposed host galaxies of repeating fast radio burst sources detected by CHIME/FRB

Ibik, Adaeze L.; Drout, Maria R.; Gaensler, B. M.; Scholz, Paul; Michilli, Daniele; Bhardwaj, Mohit; Kaspi, Victoria M.; Pleunis, Ziggy; Cassanelli, Tomas; Cook, Amanda M.; Dong, Fengqiu A.; Kaczmarek, Jane F.; Leung, Calvin; Lu, Katherine J.; Masui, Kiyoshi W.; Pearlman, Aaron B.; Rafiei-Ravandi, Masoud; Sand, Ketan R; Shin, Kaitlyn; Smith, Kendrick M.; Stairs, Ingrid H.

This publication could be one of several versions: author's original, accepted manuscript or the publisher's version. / La version de cette publication peut être l'une des suivantes : la version prépublication de l'auteur, la version acceptée du manuscrit ou la version de l'éditeur.
For the publisher's version, please access the DOI link below./ Pour consulter la version de l'éditeur, utilisez le lien DOI ci-dessous.

Publisher's version / Version de l'éditeur:
https://doi.org/10.3847/1538-4357/ad0893
The Astrophysical Journal, 961, 1, pp. 1-17, 2024-01-17

NRC Publications Archive Record / Notice des Archives des publications du CNRC :
https://nrc-publications.canada.ca/eng/view/object/?id=bdccee1b-b307-4035-af4e-1f66ab234df9
https://publications-cnrc.canada.ca/fra/voir/objet/?id=bdccee1b-b307-4035-af4e-1f66ab234df9

Access and use of this website and the material on it are subject to the Terms and Conditions set forth at
https://nrc-publications.canada.ca/eng/copyright
READ THESE TERMS AND CONDITIONS CAREFULLY BEFORE USING THIS WEBSITE.

L'accès à ce site Web et l'utilisation de son contenu sont assujettis aux conditions présentées dans le site
https://publications-cnrc.canada.ca/fra/droits
LISEZ CES CONDITIONS ATTENTIVEMENT AVANT D'UTILISER CE SITE WEB.

Questions? Contact the NRC Publications Archive team at PublicationsArchive-ArchivesPublications@nrc-cnrc.gc.ca. If you wish to email the authors directly, please see the first page of the publication for their contact information.

Vous avez des questions? Nous pouvons vous aider. Pour communiquer directement avec un auteur, consultez la première page de la revue dans laquelle son article a été publié afin de trouver ses coordonnées. Si vous n'arrivez pas à les repérer, communiquez avec nous à PublicationsArchive-ArchivesPublications@nrc-cnrc.gc.ca.

National Research Council Canada | Conseil national de recherches Canada

Canada

The Astrophysical Journal, 961:99 (17pp), 2024 January 20 https://doi.org/10.3847/1538-4357/ad0893
© 2024. The Author(s). Published by the American Astronomical Society.
OPEN ACCESS

Proposed Host Galaxies of Repeating Fast Radio Burst Sources Detected by CHIME/FRB

Adaeze L. Ibik[1,2], Maria R. Drout[1,2], B. M. Gaensler[1,2,3], Paul Scholz[2], Daniele Michilli[4,5], Mohit Bhardwaj[6], Victoria M. Kaspi[7,8], Ziggy Pleunis[2], Tomas Cassanelli[9], Amanda M. Cook[1,2], Fengqiu A. Dong[10], Jane F. Kaczmarek[11,12], Calvin Leung[4,5], Katherine J. Lu[6], Kiyoshi W. Masui[4,5], Aaron B. Pearlman[7,8], Masoud Rafiei-Ravandi[7,8], Ketan R Sand[7,8], Kaitlyn Shin[4,5], Kendrick M. Smith[13], and Ingrid H. Stairs[10]
[1] David A. Dunlap Department of Astronomy & Astrophysics, University of Toronto, 50 St. George Street, Toronto, ON M5S 3H4, Canada; adaeze.ibik@mail.utoronto.ca
[2] Dunlap Institute for Astronomy & Astrophysics, University of Toronto, 50 St. George Street, Toronto, ON M5S 3H4, Canada
[3] Present address: Division of Physical and Biological Sciences, University of California Santa Cruz, 1156 High Street, Santa Cruz, CA 95064, USA
[4] MIT Kavli Institute for Astrophysics and Space Research, Massachusetts Institute of Technology, 77 Massachusetts Avenue, Cambridge, MA 02139, USA
[5] Department of Physics, Massachusetts Institute of Technology, 77 Massachusetts Avenue, Cambridge, MA 02139, USA
[6] Department of Physics, Carnegie Mellon University, 5000 Forbes Avenue, Pittsburgh, 15213, PA, USA
[7] Department of Physics, McGill University, 3600 rue University, Montréal, QC H3A 2T8, Canada
[8] Trottier Space Institute, McGill University, 3550 rue University, Montréal, QC H3A 2A7, Canada
[9] Department of Electrical Engineering, Universidad de Chile, Av. Tupper 2007, Santiago 8370451, Chile
[10] Department of Physics and Astronomy, University of British Columbia, 6224 Agricultural Road, Vancouver, BC V6T 1Z1 Canada
[11] Dominion Radio Astrophysical Observatory, Herzberg Research Centre for Astronomy and Astrophysics, National Research Council Canada, P.O. Box 248, Penticton, BC V2A 6J9, Canada
[12] CSIRO Astronomy and Space Science, Parkes Observatory, P.O. Box 276, Parkes NSW 2870, Australia
[13] Perimeter Institute for Theoretical Physics, 31 Caroline Street N, Waterloo, ON N25 2YL, Canada
Received 2023 April 3; revised 2023 October 27; accepted 2023 October 30; published 2024 January 17

Abstract

We present a search for host galaxy associations for the third set of repeating fast radio burst (FRB) sources discovered by the CHIME/FRB Collaboration. Using the $\sim 1'$ CHIME/FRB baseband localizations and probabilistic methods, we identify potential host galaxies of two FRBs, 20200223B and 20190110C at redshifts of 0.06024(2) and 0.12244(6), respectively. We also discuss the properties of a third marginal candidate host galaxy association for FRB 20191106C with a host redshift of 0.10775(1). The three putative host galaxies are all relatively massive, fall on the standard mass–metallicity relationship for nearby galaxies, and show evidence of ongoing star formation. They also all show signatures of being in a transitional regime, falling in the *green valley*, which is between the bulk of star-forming and quiescent galaxies. The plausible host galaxies identified by our analysis are consistent with the overall population of repeating and nonrepeating FRB hosts while increasing the fraction of massive and bright galaxies. Coupled with these previous host associations, we identify a possible excess of FRB repeaters whose host galaxies have $M_u - M_r$ colors redder than the bulk of star-forming galaxies. Additional precise localizations are required to confirm this trend.

Unified Astronomy Thesaurus concepts: Radio transient sources (2008); Radio bursts (1339)

1. Introduction

Over 600 short-duration energetic radio pulses known as fast radio bursts (FRBs; Lorimer et al. 2007) have been reported[14] (CHIME/FRB Collaboration et al. 2021; Nimmo et al. 2023). Multiple FRBs that are coincident in sky location and dispersion measure (DM)—*FRB repeaters*—are particularly interesting since they provide more opportunities for detailed follow-up studies. While we do not yet know whether repeaters and one-off FRBs are two separate classes, the existence of repeaters demonstrates that the progenitors of at least some FRBs are not cataclysmic (for a review of FRB models, see Platts et al. 2019). Recently, the magnetar theory for FRBs (Beloborodov 2017; Metzger et al. 2019) was confirmed as one possible origin of FRB with the discovery of a very luminous FRB-like burst from the Galactic magnetar SGR 1935+2154 (Bochenek et al. 2020; CHIME/FRB Collaboration et al. 2020). However, it remains the only FRB source confirmed to be a magnetar, emphasizing the need for additional probe of their nature.

The host galaxies of various types of transients have often provided useful insight into their origins—allowing constraints on the ages and physical properties required to produce them (e.g., Eftekhari et al. 2019, 2021). To date, approximately 39 (Nimmo & Chatterjee 2023) FRBs have been localized to their host galaxies (e.g., Chatterjee et al. 2017; Bhandari et al. 2020, 2022a, 2023; Heintz et al. 2020; Bhardwaj et al. 2021b; Niu et al. 2022; Michilli et al. 2023; Rajwade et al. 2022; Driessen et al. 2024; Gordon et al. 2023; Jankowski et al. 2023; Sharma et al. 2023). This is due to the difficulty of pinpointing FRBs within the arcsecond precision required for robust host associations (Eftekhari & Berger 2017) and multiwavelength follow-up (e.g., Scholz et al. 2017). The host populations of both repeating and nonrepeating FRBs have diverse properties (star-forming or quiescent, low or high metallicity, massive or dwarf, spiral or elliptical; e.g., Heintz et al. 2020; Bhandari et al. 2022a, 2022b), and it is not clear what type of host is

[14] https://www.chime-frb.ca/catalog

Original content from this work may be used under the terms of the Creative Commons Attribution 4.0 licence. Any further distribution of this work must maintain attribution to the author(s) and the title of the work, journal citation and DOI.

preferred by repeaters. While the nature and the origin of repeating FRBs are still debated, finding more host galaxies will provide insights into the origin of the FRB population. In addition to understanding the nature of FRBs, FRBs with known host galaxies are useful cosmological probes because the relationship between their DMs and redshifts could give insight into the missing baryons in the intergalactic medium (IGM; Macquart et al. 2020).

Recently, the Canadian Hydrogen Intensity Mapping Experiment Fast Radio Burst (CHIME/FRB) project (CHIME/FRB Collaboration et al. 2018) published 25 new repeaters and a further 14 candidates as described by CHIME/FRB Collaboration & Andersen (2023). This supplements 21 previously published CHIME/FRB repeaters (CHIME/FRB Collaboration et al. 2019a, 2019b; Fonseca et al. 2020; Bhardwaj et al. 2021a; Lanman et al. 2022; Mckinven & CHIME/FRB Collaboration 2022), all of which are observed in the frequency range 400–800 MHz. This sample represents by far the largest population of repeaters detected by a single survey to date and thus offers the opportunity to learn about various properties of the FRB population. CHIME/FRB repeaters show a lower average DM than those of apparently nonrepeating sources (CHIME/FRB Collaboration & Andersen 2023) even though this could be a selection effect (see Connor et al. 2020).

Other previously established characteristic properties of repeaters such as wider bursts and narrower emitting bandwidths than nonrepeating FRBs were confirmed in the additional set of repeaters (CHIME/FRB Collaboration et al. 2021; Pleunis et al. 2021). These observational differences could signal a distinct astrophysical origin for repeaters. Additional multiwavelength studies with a larger sample, including host galaxy identification, could help to disentangle potential multiple populations.

Typically, robust host associations require $\lesssim 1''$ localizations for the FRBs, and hence detection of a burst with interferometers (Eftekhari & Berger 2017). Indeed, some FRB repeaters (e.g., FRB 20180916B and 20201124A; Marcote et al. 2020; Nimmo et al. 2022) discovered by CHIME/FRB have subsequently been associated with their host galaxies by means of very long-baseline interferometry (VLBI). However, arcsecond localizations are not available for most CHIME/FRB bursts. At best, CHIME/FRB can achieve $\sim 1'$ localization for bursts when baseband data are recorded. CHIME/FRB baseband data are channelized raw voltages of the FRB signals from the telescope feeds. Localizations with precision $\sim 1'$ using baseband data from CHIME/FRB can be obtained following the techniques described by Michilli et al. (2021). While these baseband positions are larger than the size of a typical galaxy in the sky, for objects in the relatively nearby universe, it is possible to make probable host galaxy associations due to the low density of galaxies at lower redshifts. This technique has previously been used to associate five FRBs detected by CHIME/FRB with likely hosts: FRBs 20200120E (Bhardwaj et al. 2021a), 20181030A (Bhardwaj et al. 2021b), 20220912A (Mckinven & CHIME/FRB Collaboration 2022), 20180814A, and 20190303A (Michilli et al. 2023), and the reliability of the method was supported by the eventual VLBI confirmation of the host galaxies for FRB 20200120E (Kirsten et al. 2022).

Future telescopes such as the CHIME/FRB Outrigger project (currently under construction) will be able to improve the number of precisely localized FRBs (Leung et al. 2021; Cassanelli et al. 2022; Mena-Parra et al. 2022). Other such facilities include the real-time fast (realfast) transients at the Karl Janskly Very Large Array (VLA; Law et al. 2018), the fast radio transient-detection program at MeerKAT (MeerTRAP; Rajwade et al. 2022), and the Deep Synoptic Array (DSA-110; Ravi et al. 2023). Until subarcseconds localization is possible for CHIME/FRB events, the baseband position remains a useful technique for associating local universe FRBs to their host galaxies (Michilli et al. 2023).

In this paper, we perform a search for likely host galaxies for 20 repeaters and 3 repeater candidates from the recently published sample by CHIME/FRB Collaboration & Andersen (2023) for which ∼arcmin baseband localization were available. In total, we identify highly probable hosts for two FRBs and one marginally significant candidate host for a third. A thorough description of our search for the probable hosts of the events is described in Section 2, and the details of the observations of likely hosts are explained in Section 3. The observed and inferred properties of the hosts are described in Section 4 including a comparison between the three hosts and previously known hosts of FRBs in Section 4.5. Finally, we summarize the result of the host associations in Section 5.

2. Search for Probable Host Galaxies

Here, we describe the process used to search for probable host galaxies to the CHIME/FRB repeaters. Specifically, after describing our initial sample (Section 2.1), we determine the maximum redshift for each FRB based on its DM (Section 2.2), search archival optical catalogs for galaxies within the localization regions for each burst (Section 2.3), and perform a probability of chance coincidence analysis (Section 2.4). Finally, we summarize these results for three galaxies identified as potential hosts to CHIME repeating FRBs in Section 2.5.

2.1. Initial FRB Sample

Of the 25 "gold" and 14 "silver" repeating FRBs presented by CHIME/FRB Collaboration & Andersen (2023), we first restrict ourselves to objects that have baseband localizations for multiple bursts because of their small localization uncertainties. This criterion is met for 20 gold and 3 silver candidates. From there, we continue the analysis with events that are in the survey coverage area of either the Sloan Digital Sky Survey (SDSS) DR12 (Alam et al. 2015) or Dark Energy Spectroscopy Instrument (DESI), Data Release 9 (DR9; Dey et al. 2019) Legacy Imaging Survey photometric catalog, as these are required to assess the population of possible host galaxies within the CHIME/FRB localizations regions. This reduced the sample list to the 12 gold and 1 silver (FRB 20190303D) candidates listed in Table 1.

2.2. Determination of z_{max}

To begin, we calculate the maximum redshift for each FRB in our sample. This is possible because the DM measured for each burst gives us an integrated column density of electrons along the line of sight. This DM will contain contributions from materials in the Milky Way (MW) disk and halo, the intergalactic medium (IGM), the host galaxy interstellar medium, and potentially the local material around the FRB. However, if electrons in the IGM are the dominant

Table 1
Summary of FRB Repeater Candidates Searched for Likely Host Galaxies

FRB Name	DM (pc cm^{-3})	DM$_{MW}$[c] (pc cm^{-3})	z_{max}	N_s[d]	Max P_{PATH}[e] $P(U) = 0.0$	Max P_{PATH}[e] $P(U) = 0.1$	$m_{r,gal}$[f] (AB mag)	$P_{cc,gal}$[g]
FRB 20200223B	201.8(4)	45.6	0.19	7	0.994	0.899	16.08	0.010
FRB 20191106C	332.2(7)	25.0	0.36	11	0.951	0.815	17.31	0.063
FRB 20190110C	221.6(1.6)	37.1	0.22	9	0.918	0.779	18.00	0.102
FRB 20190804E	363.2(3)	43.4	0.37	9	0.638	0.549	19.13	0.305
FRB 20200118D	625.7(1.4)	76.6	0.62	14	0.619	0.520	19.71	0.491
FRB 20201114A	321.1(8)	37.8	0.33	60	0.537	0.454	17.68	0.469
FRB 20200913C	574.2(1.6)	47.8	0.60	74	0.490	0.407	17.87	0.600
FRB 20200929C	413.3(3)	38.4	0.44	41	0.474	0.388	17.04	0.144
FRB 20191013D	524.1(6.5)	43.1	0.55	111	0.465	0.396	17.49	0.401
FRB 20190609C[a]	479.2(3)	113.4	0.43	3	0.409	0.354	22.58	0.745
FRB 20201221B	509.5(1.1)	50.9	0.53	45	0.210	0.175	19.48	0.686
FRB 20190303D[b]	716.6(1.6)	36.5	0.77	28	0.118	0.098	20.55	0.750
FRB 20200619A	439.6(0.4)	50.8	0.45	350	0.080	0.067	18.18	0.753

Notes.
[a] PATH probability using the SDSS list of host candidates while others used the DESI list of host candidates.
[b] This is the only silver candidate in our sample. The rest of the candidates are from the gold sample.
[c] DM contribution expected for the disk of the Milky Way from the NE2001 model (Cordes & Lazio 2002).
[d] N_s is the number of extended optical objects detected in the FRB 90% error region.
[e] Max P_{PATH} is the maximum probability estimated by PATH for each FRB region given two different priors, $P(U) = 0.0$, and $P(U) = 0.1$. FRBs are ordered in the decreasing order of Max P_{PATH}.
[f] $m_{r,\ gal}$(AB) is the r-band AB magnitude of the plausible host of the FRB as identified by PATH.
[g] $P_{cc,gal}$ is the probability of finding a galaxy with the r-band magnitude of the most probable host or brighter ($<m_{r,\ gal}$) within each FRB 90% error region.

contribution, the DM of FRBs is approximately linearly related to redshift.

For each of the FRBs in Table 1, we determine the maximum redshift z_{max} using DMs taken from CHIME/FRB Collaboration & Andersen (2023). To do this, we subtract the DM contribution expected for the disk of the MW from the NE2001 model (Cordes & Lazio 2002), DM$_{MW}$(NE2001), but do not attempt to correct for contributions from either the MW halo (DM$_{halo}$) or the FRB host galaxy (DM$_{host}$).

This method provides us with a conservative estimate for the *excess* DM associated with each burst (DM$_{excess}$). We then calculate the maximum redshift, z_{max}, for each repeater event by attributing this entire DM$_{excess}$ to the IGM using the FRUITBAT software (Batten 2019). FRUITBAT uses the given DM to estimate the maximum redshift given the cosmology of Komatsu et al. (2009) and the DM-redshift relationship of Zhang (2018). In Table 1, we list the DM, DM$_{MW}$(NE2001), and z_{max} for all bursts in our sample. The derived z_{max} values span $0.19 < z_{max} < 0.77$.

We acknowledge that this method is different from that described by Bhardwaj et al. (2021a) and used in other CHIME/FRB papers. However, we emphasize that z_{max} is not utilized in the probabilistic analysis below. We consider all galaxies in the field of the FRB. Rather, z_{max} is only used to ensure that any individual host with a high probability of association has $z < z_{max}$ (see Section 2.5). However, using the method described by Bhardwaj et al. (2021a) does not change the set of possible host galaxies. We, therefore, opt for the most conservative approach.

2.3. Optical Galaxy Catalog Search

We searched the SDSS and DESI catalogs for host galaxy candidates within the 90%-confidence baseband positions of the FRBs. For 12 of the 13 events that are in the survey coverage area of both DESI and SDSS, we adopted the DESI catalog, which is more sensitive to fainter sources (r-band 5σ depths of ∼23.4 mag), while the SDSS catalog (r-band 5σ depths of ∼22.7 mag) was used to analyze FRB 20190609C. The impact of completeness in these catalogs, especially for faint galaxies, will be discussed below. To identify likely host galaxies, we first exclude any object classified as a point source within the SDSS or DESI catalogs. Multiple extended sources were found within the 90%-confidence positional error region for each FRB. We record the number of extended objects within the localization regions for each FRB as N_s in Table 1.

2.4. Host Probability Analysis

We use two complementary methods to assess the likelihood that a galaxy within the CHIME/FRB error region can be robustly associated with a host galaxy. We use the result of these methods together to decide on when or whether likely host associations can be made.

First method. First, for the cases where more than one galaxy was identified in DESI/SDSS imaging, we analyze the probability of each being associated with the FRB using the formalism described in the Probabilistic Association of Transients to their Hosts (PATH) software (Aggarwal et al. 2021). PATH takes as input the FRB position and its uncertainty, and the r-band magnitudes and half-light radii of all candidate galaxies. It then calculates a probability for each galaxy using Bayes' theorem and accounting for the FRB localization error region. We initially adopt priors that assume (i) the probability that each candidate galaxy is the host and is inversely proportional to the angular surface density of galaxies with magnitudes equal to or brighter than the candidate's magnitude (based on galaxy counts from Driver et al. 2016), (ii) the probability of finding the host galaxy of the FRB at a given physical offset is an exponentially declining function, and (iii) that the probability that the true host was undetected, $P(U)$, was zero ($P(U) = 0$). The impact of adjusting this final

assumption on the resultant probabilities is examined below, as well as how reasonable the assumption is given the depth of the DESI/SDSS surveys at the maximum redshifts of specific bursts (see Section 2.5). For the CHIME/FRB host candidates described above, we obtained the half-light radii in arcseconds from DESI and used the Petrosian radius instead in the absence of a half-light radius for the FRB with only SDSS data.

Applying the PATH framework, we obtain a probability of associating the FRB with each of the candidates identified in its localization region and report the highest probability value, Max $P_{\rm PATH}$ in Table 1. In total, we find three FRBs where the maximum PATH probability ($P_{\rm PATH}$) for the $P(U) = 0$ case is $> 90\%$. Given that we initially ran PATH adopting a probability of zero that the true host was undetected (and hence not in our candidate list), this is effectively a statement that PATH significantly prefers one of the candidate hosts over all *detected* galaxies.[15] For the remaining 10 FRBs, PATH gives a maximum probability to any individual galaxy of $\lesssim 75\%$ *even* in the case that the probability of an undetected host is zero. For these cases, we argue that it is not possible to make a likely host association with current data, while the three FRBs with higher Max $P_{\rm PATH}$ warrant further examination.

In particular, it is possible that some potential host galaxies were missing from our initial candidate lists. The DESI detection limit corresponds to an absolute r-band magnitude of -15.9 to -17.48 at redshifts between 0.19 and 0.36 (the range of $z_{\rm max}$ values for the three bursts with the highest PATH probability hosts). At these depths, we are sensitive to galaxies fainter than $0.1L_*$ including all of the superluminous supernova and long-duration gamma-ray burst host galaxies at $z < 0.3$ of Lunnan et al. (2014). However, some of the faintest dwarf galaxies, such as the $M_r > -16.5$ host of FRB121102 (Chatterjee et al. 2017), could have eluded detection at the high-end of this distance range.

Given the possibility of undetected dwarf galaxies, we rerun PATH, now setting an arbitrary prior on the probability that the true host was undetected as $P(U) = 0.1$ (recommended by the authors of PATH). The results are also listed in Table 1. For one FRB, 20200223B, the galaxy with the maximum PATH probability is approximately 90%, while, for the other two (20190110C, 20191106C), the maximum PATH probability falls to 82%–78%. We will further discuss the appropriateness of these values of *P(U)* for each of these specific FRBs—given our survey depth at their maximum distance—in Section 2.5.

Second method. Given that the appropriate value for $P(U)$ for each burst is uncertain, we also calculate the probability that the galaxy *most preferred by PATH* would be found within the CHIME localization region for that FRB by chance. To calculate this probability of chance coincidence ($P_{\rm cc,gal}$), we use a Monte Carlo approach. Specifically, for each FRB, we query random patches of the sky within the SDSS footprint having the size of the FRB localization region for 1000 times. We used SDSS instead of DESI because it was easier to query the entire SDSS catalog multiple times for many error regions. We determine the number of galaxies within that patch that have r-band magnitudes brighter than or equal to that of the most probable host galaxy according to PATH ($m_r \leqslant m_{r,\rm gal}$). We then use the fractions of these runs that have at least one galaxy that meets this requirement to determine the probability that the most plausible identified host was within the FRB 90%-confidence localization region by chance. In Table 1, we list $P_{\rm cc,gal}$ as well as the AB r-band magnitude ($m_{r,\rm gal}$) values for the preferred host of these FRBs.

We note that these values are most useful in cases where the maximum PATH probability is high. For example, while the galaxy with the highest PATH probability within the localization region of FRB 20200929C has a small $P_{\rm cc,gal}$ of 14.4%, PATH only assigns a probability of ∼38%–47% that this is the true host because there are two galaxies of similar brightness within the localization region. On the other hand, for three FRBs (20200223B, 20190110C, 20191106C) with maximum PATH probability at $P(U) = 0 > 90\%$, we calculate that there was a $\leqslant 10\%$ chance that the preferred galaxy is located within the CHIME/FRB localization region by chance.

We emphasize that these $P_{\rm cc,gal}$ values describe the probability that an *individual* galaxy would be located within an area the size of an *individual* FRB localization region. They do not account for *look-elsewhere* effects associated with the fact that we have searched multiple CHIME/FRB localization regions as part of this overall study. If we instead perform our Monte Carlo analysis considering a region with the *combined* area of all 13 FRBs listed in Table 1, we find the following: (i) in 71.7% of trials, there is at least one galaxy with $m_r < 16.28$ (the SDSS magnitude of the preferred host for FRB 20200223B), (ii) in 72.9% of trials, there are at least 3 galaxies with $m_r < 17.43$ (the SDSS magnitude of the preferred host for FRB 20191106C), and (iii) in 73.6% of trials, there are at least 8 galaxies with $m_r < 18.18$ (the SDSS magnitude of the preferred host for FRB 20190110C). For cases (ii) and (iii), we quote values for at least 3 and 8 galaxies, respectively, because that was the total number of galaxies with those brightnesses found in the combined localization regions of all 13 FRBs. These numbers indicate that there is a relatively low $P_{\rm cc,gal}$ of finding a bright galaxy in the localization region of an individual FRB (e.g., 1.0% for FRB 20200223B). When considering the search region as a whole, we do not see evidence for a strong overabundance of bright galaxies within the *combined* 13 CHIME/FRB repeaters regions. This implies that we cannot make associations for our galaxies using $P_{\rm cc}$ based on galaxy number counts *alone*.

2.5. Summary of Possible Host Associations

In the analysis above, we identified three galaxies that we felt were worthy of further investigation due to PATH strongly preferring an individual galaxy over any other source *detected* in the field. We found that when *look-elsewhere* effects were considered, there is not a *strong* overabundance of bright galaxies ($m_r < 18$ mag) within the 13 combined CHIME/FRBs localization regions. However, if we assume that FRBs must come from galaxies, then the Bayesian approach of PATH—which takes into account not only galaxy number counts but also information on transients offsets—offers a means to robustly consider the relative probabilities of possible hosts for an individual FRB. We, therefore, rely primarily on the PATH analysis. Here, we synthesize information available for the three galaxies necessary to infer whether a likely host association can be made.

FRB 20200223B. There are seven extended sources in the DESI catalog in the field of FRB 20200223B. These are marked as green boxes in the left panel of Figure 1, and have apparent r-band magnitudes in the range $16.08 < m_r < 23.97$. The morphology of Source 1 suggests a spiral galaxy while

[15] The resulting PATH probabilities for all galaxies within these fields are given in Appendix.

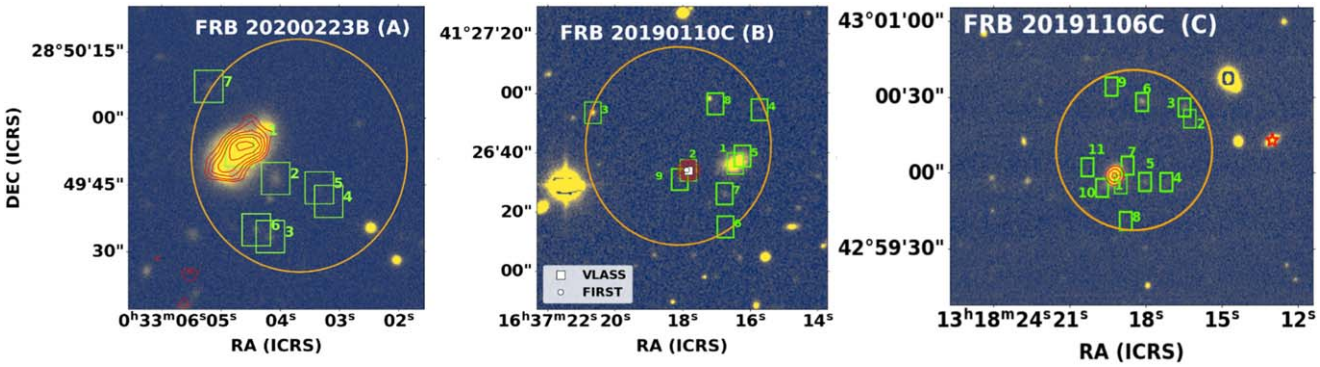

Figure 1. DESI *r*-band images showing the 90% baseband localization region of FRBs 20200223B, 20190110C and 20191106C (orange ellipses). Green boxes show the positions of host galaxy candidates. The red background contours are from high-resolution LOFAR Two-meter Sky Survey (LoTSS; Shimwell et al. 2022) radio data. Left: FRB 20200223B; there are 7 sources within the localization region from the DESI catalog. galaxy A, marked as 1 in the image, is a spiral galaxy at $z_{\rm spec} = 0.06$ and is the most plausible host galaxy of FRB 20200223B. The red background contours from LoTSS fit the morphology of A and are thus consistent with star formation activities of the galaxy. Middle: FRB 20190110C; we present 9 sources from the DESI catalog in this FRB region. Galaxy B, marked as 1, is the plausible host galaxy of FRB 20190110C at $z_{\rm spec} = 0.122$. The white markers represent VLASS and FIRST radio point sources in the field of the FRB spatially coincident with another nearby galaxy named Source 2. There is no radio source that is coincident with galaxy B. Right: FRB 20191106C; there are 11 sources within the localization region from the DESI catalog. Source 1 (C) is a galaxy at $z_{\rm spec} = 0.108$ and is the most likely host of FRB 20191106C. There is a LoTSS radio source just outside the region shown as a red star, but the one that is spatially coincident with galaxy C is shown as a red contour.

Sources 2–7 are faint objects in the field. Of these, Source 1 (SDSS J003304.68+284952.6; hereafter A) with m_r(AB) = 16.080 ± 0.001 mag and an effective radius of $5\farcs81 \pm 0\farcs02$ is the galaxy preferred by PATH (see Table A1 in the Appendix for PATH probabilities assigned to all galaxies in the field of this FRB).

When adopting $P(U) = 0$, PATH gives a probability of 99.4% that the FRB is associated with galaxy A (Table 1). Given that the DESI depth corresponds to an absolute magnitude of roughly −15.90 mag at $z_{\rm max} < 0.19$, our initial search should have been sensitive to all FRB hosts discovered to date. The probabilities obtained using the prior, $P(U) = 0$, are likely reasonable for this FRB. In addition, we found that the probability of finding an $m_r = 16.1$ mag galaxy in the CHIME localization region for FRB 20200223B by chance was ∼1.0%.

Finally, we note that the photometric redshift for this galaxy ($z_{\rm phot} = 0.06 \pm 0.01$) is less than $z_{\rm max}$ for this FRB ($z_{\rm max} < 0.19$). We, therefore, consider this host association robust. A is located at α(J2000) = $00^{\rm h}33^{\rm m}04\fs68$ ($0\farcs015$), and δ(J2000) = $+28°49'52\farcs60$ ($0\farcs021$; Alam et al. 2015).

FRB 20190110C. We found nine objects that are not point sources in the field of FRB 20190110C by searching the DESI DR9 catalog (shown in green boxes on the middle panel of Figure 1). The nine sources have apparent DESI *r*-band magnitudes in the range $18.0 < m_r < 23.9$. By visual inspection, Source 1 looks like an irregularly shaped object with an extended clump classified as Source 5 by DESI. We, therefore, consider them the same as opposed to distinct sources. Source 1, SDSS J163716.43+412636.2 (hereafter B), has a probability of being associated with the FRB of $P_{\rm PATH} = 91.8\%$ (when adopting $P(U) = 0$), and has a $z_{\rm phot} = 0.10 \pm 0.02$ compared to $z_{\rm max} < 0.22$ for this target. It has apparent *r*-band magnitude, m_r(AB) 18.009 ± 0.006, and an effective radius of $3\farcs38 \pm 0\farcs03$.

The DESI depth of m_r(AB) ∼24 mag corresponds to an absolute magnitude of roughly −16.26 mag at $z_{\rm max} < 0.22$, and thus, we were sensitive to all FRB hosts discovered to date. Given this, the probabilities obtained using the prior, $P(U) = 0$, is likely reasonable for this FRB. In addition, we found that the probability of finding an $m_r = 18.0$ mag galaxy in the CHIME localization region by chance was 10.2%. We, therefore, conclude that B is the likely host galaxy of FRB 20190110C. Galaxy B is located at α(J2000) = $16^{\rm h}37^{\rm m}16\fs43$ ($0\farcs022$), and δ(J2000) = $+41°26'36\farcs30$ ($0\farcs024$; Alam et al. 2015). We report the PATH probability of all the sources in the field of this FRB in Table A2 of the Appendix.

FRB 20191106C. 11 objects that are not point sources were found in the DESI catalog within the baseband region of FRB 20191106C. See the green boxes in Figure 1. The eleven sources have apparent DESI *r*-band magnitudes in the range $17.3 < m_r < 23.9$.

We note that the DM for FRB 20191106C is larger than those of the other two FRBs discussed in this section, leading to a higher $z_{\rm max}$. As a result, the DESI limit corresponds to a slightly higher absolute magnitude of roughly −17.48 mag at $z_{\rm max} < 0.36$, and it is possible that some dwarf galaxies were missing from our initial candidate list (for example, the known host of FRB 121102 at −16.5 mag; Chatterjee et al. 2017). Given these, it is likely more appropriate to use $P(U) = 0.1$ for this FRB.

Even when adopting $P(U) = 0.1$, PATH significantly prefers Source 1 (SDSS J131819.23+425958.9, hereafter C) over any other objects in the field. It assigns a probability of 81.5% to galaxy C compared to $\lesssim$1% for any other galaxy in the field (see Table A3 in the Appendix where we report the PATH probability of all the sources in the field of this FRB). However, we found that the probability of finding an $m_r = 17.3$ mag galaxy in the CHIME localization region by chance is 6.3%. Therefore, we argue that C is likely a good candidate host of the FRB. It is located at α(J2000) = $13^{\rm h}18^{\rm m}19\fs23$ ($0\farcs01$), and δ(J2000) = $+42°59'58\farcs97$ ($0\farcs01$; Alam et al. 2015) and looks like an elliptical or irregular galaxy with m_r(AB) of 17.306 ± 0.003.

Summary. Based on the results above, we conclude that galaxies A and B are highly probable hosts for FRB 20200223B and FRB 20190110C, respectively. Both galaxies have >90% probability of being the true host based on PATH, and the depth of the archival surveys is sufficient to detect all previously discovered FRB host galaxies. As described above, although it is not possible to make host associations based on galaxy number counts in the 13 CHIME/FRB localization

regions alone, if we assume that FRBs come from galaxies, the Bayesian approach of PATH provides a means to assess the most likely host. In contrast, the association of galaxy C to FRB 20191106C is more marginal due to the shallower depth of archival surveys, which means that the probability of unseen galaxies as the host is nonnegligible. This leads to a PATH probability below 90% when adopting a value of *P(U)* that is greater than 0. However, given that PATH strongly preferred this host over any other source found in the field, we chose to also describe the properties of this galaxy in the section below.

Finally, we note that the FRB host galaxy association method described in this manuscript is different from that used in previously published CHIME/FRB papers (Bhardwaj et al. 2021a, 2021b; Michilli et al. 2023). The latter involves obtaining spectroscopic redshifts of all the galaxy candidates within the FRB field and uses the $z_{\rm spec} < z_{\rm max}$ condition to decide on host association. Given that we are looking at many FRB fields, some of which have high DMs, it is beyond the scope of the present work to conduct spectroscopic analysis for all the candidates in each field. Hence, we adopt the probabilistic method as described here. However, future more detailed studies involving spectroscopic redshifts could be of use.

3. Observations of Likely Host Associations

Here, we describe the full set of archival and follow-up observations obtained for the plausible host galaxies of FRBs 20200223B, 20191106C, and 20190110C. These will be used to measure detailed host properties in Section 4.

3.1. Optical and Infrared Photometry

We retrieved photometric data for each of the 3 host galaxies from SDSS, DESI, the Wide-field Infrared Survey Explorer (WISE; Wright et al. 2010), Two Micron All Sky Survey (2MASS; Cutri et al. 2003), the Galaxy Evolution Explorer (GALEX; Bianchi et al. 2017), and the Spitzer Enhanced Imaging Product source list (Spitzer Science Center (SSC) & Infrared Science Archive (IRSA), 2021). We will use these optical-infrared spectral energy distributions (SEDs) to estimate various properties of the galaxies in Section 4.2. We corrected all data for Galactic foreground extinction using the dust reddening map of Schlegel et al. 1998 and assuming an $R_{\rm v} = 3.1$ MW extinction curve. $E(B-V)$ values are 0.0489 (8), 0.0081(5), and 0.0200(8) for galaxies A, B, and C respectively.

The infrared colors of galaxies A, B, and C in the WISE bands can be seen in Figure 2. Using the WISE color-map diagnostic plot (Wright et al. 2010; Nikutta et al. 2014), galaxy A falls in a region also occupied by spiral, star-forming, starburst, low-ionization nuclear emission-line regions galaxies, and luminous infrared galaxies (LIRG; Jarrett et al. 2017). While the morphology of galaxy B is ambiguous, the infrared colors also overlap with spiral galaxies and LIRGs, implying a star-forming galaxy. Finally, we note that galaxy C was previously classified as an elliptical galaxy by Kuminski & Shamir (2016) with ∼88% certainty and an ellipticity of 0.4 (Simard et al. 2011). However, the infrared colors overlap with various classes of star-forming galaxies (spiral, starburst, and LIRGs), which is inconsistent with a typical quiescent elliptical galaxy. Moreover, this infrared color result is in line with the result of Ellison et al. (2016) who use artificial neural networks to model the total infrared luminosity, where they predict that C is a star-forming galaxy. We conclude that C could be among the rare population of elliptical galaxies with ongoing star formation.

3.2. Optical Spectroscopy

For all three likely host galaxies, we use optical spectroscopy to determine their spectroscopic redshifts and emission line fluxes—particularly, H_α, H_β, [O III](λ5006 Å), and [N II] (λ6582 Å)—that will then be used to estimate other galaxy properties in Section 4.1. In all cases, we convert redshifts to luminosity distances assuming a flat $\Lambda_{\rm CDM}$ cosmology with $H_0 = 67.7$ km s^{-1} Mpc^{-1}, $\Omega_{\rm m} = 0.31$, and $\Omega_\wedge = 0.70$ (Planck Collaboration et al. 2020).

3.2.1. Archival Spectroscopy

For galaxies A and C, archival spectra are available. For FRB 20200223B, the likely host galaxy, A, was observed and released as part of the Large Sky Area Multi-Object Fiber Spectroscopic Telescope (LAMOST; Cui et al. 2012) Data Release 5 (DR5). We retrieve the redshift and relevant emission line fluxes. The spectroscopic redshift is $z_{\rm spec} = 0.06024(2)$, which corresponds to a luminosity distance of 278.97(9) Mpc. For FRB 20191106C, the likely host galaxy, C, was observed as part of SDSS DR12, and the redshift was reported by Alam et al. (2015). The spectroscopic redshift is $z_{\rm spec} = 0.10775(1)$, which corresponds to a luminosity distance of 515.32(4) Mpc. The emission line fluxes for galaxy C were extracted from the SDSS-III spectroscopic survey (Eisenstein et al. 2011; Ahumada et al. 2020).

For both A and C, we correct the previously published LAMOST/SDSS line fluxes for foreground MW extinction. We determine correction factors based on the Cardelli et al. (1989) extinction law ($R_{\rm V} = 3.1$) at the rest wavelengths of H_α, H_β, [O III](λ5006 Å) and [N II](λ6582 Å). In addition, we also check for intrinsic host galaxy extinction by calculating the Balmer decrement from the H_α, H_β line fluxes. Compared to the theoretical Case-B recombination line ratio of H_α/H_β=2.86, we do not find evidence for significant additional extinction.

3.2.2. Gemini North Spectroscopy

For FRB 20190110C, there is no archival spectroscopy available for its plausible host galaxy, B. Hence, we obtained an observation with the Gemini Multi-Object Spectrograph (GMOS) of the Gemini-North telescope in Hawaii. The data were obtained on 2022 August 20 during semester 2022B. We used the 1.″0 long-slit, R400 grating and OG515 (> 520 nm) blocking filter, at central wavelengths of 720/730 nm. In total, we obtained five 1200 s exposures with a mean airmass of 1.2.

The data were reduced using the standard packages of gmos and gemini routine in PYRAF (Science Software Branch at STScI 2012). This included overscan correction, flat-fielding, sky subtraction, wavelength calibration, extraction, and flux calibration. Chip gaps and cosmic rays were removed from individual exposures, and the different exposure spectra were combined to produce a single spectrum. In order to estimate the redshift of galaxy B from the spectrum, we measured the observed central wavelengths of the H_α, H_β, [N II], and S II emission lines. We recorded a redshift of $z_{\rm spec} = 0.12244(6)$, which corresponds to a luminosity distance of 591.2(3) Mpc.

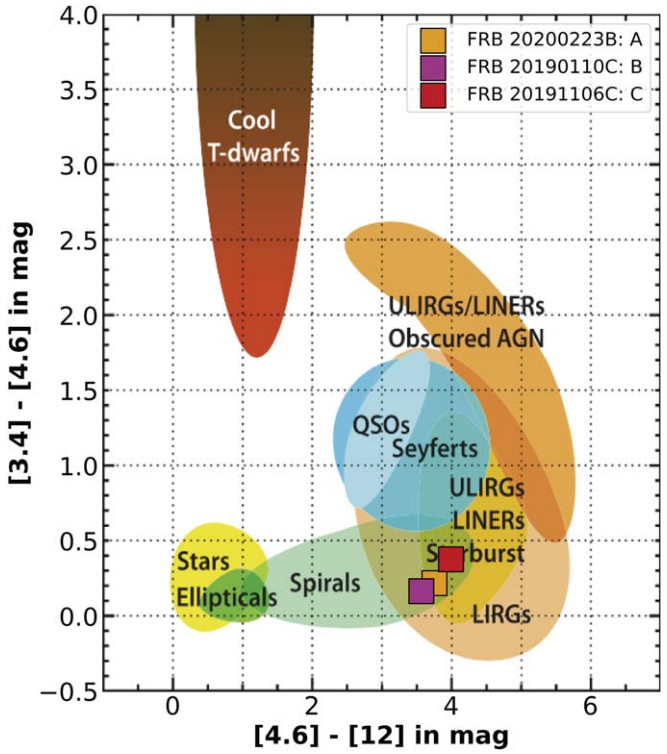

Figure 2. WISE diagnostic plot adapted from Wright et al. (2010) showing the location of various classes of objects with the 3 plausible host galaxies overplotted as orange, purple, and red squares for galaxies A, B, and C. The infrared colors from the 3 plausible host galaxies all seem to be associated with various types of star-forming galaxies.

The spectrum was then corrected for cosmological expansion using the redshift and corrected for MW extinction using the Cardelli et al. (1989) extinction law (see Figure 3). As above, we find no evidence for significant additional internal extinction when calculating the Balmer decrement. The line fluxes of H_α, H_β, [O III](λ5006 Å), and [N II](λ6582 Å) were then measured by fitting a Gaussian profile to the rest-frame spectrum. The process was carried out in an automated manner and repeated 100 times to estimate the error in the line fluxes due to uncertainty at the continuum level.

3.3. Radio Emission

We searched for the presence of a persistent radio source (PRS) within the error regions of the three FRBs using archival radio catalogs from the VLA Sky Survey (VLASS; Lacy et al. 2020), the NRAO VLA Sky Survey (NVSS; Condon et al. 1998), the Faint Images of the Radio Sky at Twenty-Centimeters (FIRST; Becker et al. 1995) survey, the TIFR-GMRT Sky Survey (TGSS; Intema et al. 2017), and the high-resolution component of the LOFAR Two-meter Sky Survey (LoTSS; Shimwell et al. 2022).

There are LoTSS radio sources at the locations of the host galaxies of FRB 20200223B and FRB 20191106C, with integrated flux densities of 2.96 ± 0.59 and 3.29 ± 0.14 mJy, respectively, at a frequency of 144 MHz. We measured upper limits on the presence of a radio source at the location of B, which is the plausible host of FRB 20190110C. In Table 2, we report detections and upper limits on radio emission in the vicinity of the plausible host galaxies from these data sets. In Section 4.3, we will investigate the possible origin of any emission detected.

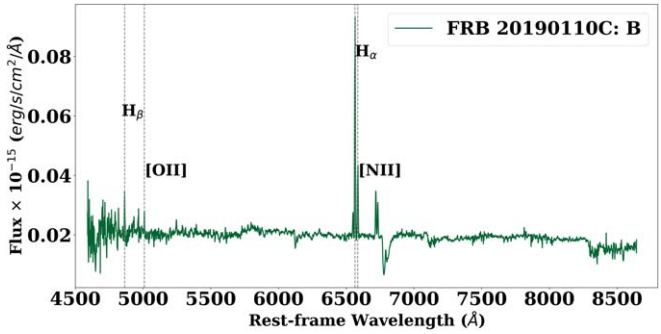

Figure 3. Gemini North spectra for the plausible host galaxy of FRB 20190110C, B. Gray lines highlight the location of prominent emission lines that were used for analysis.

4. Properties of Likely Host Associations

Here, we described the properties of galaxies A, B, and C. We investigate the implication of the results from optical spectroscopy used to estimate galaxy properties of A, B, and C in Section 4.1. We then report on the SED fitting using `Prospector` for galaxies A and B in Section 4.2, and place constraints on the presence of radio emission from these galaxies in Section 4.3. We check for any intervening structures that could contribute to the DM and discuss their effect on DM_{host} for the FRB in our sample in Section 4.4. Finally, in Section 4.5, we compare the properties of these galaxies to the hosts of other FRBs.

4.1. Optical Emission Line Diagnostics

For the three host galaxies, we use the corrected emission line fluxes (see Section 3.2) to infer their dominant source of photoionization, star formation rates, and metallicities.

BPT diagram. In order to probe the major source of photoionization in each of the three galaxies, we first placed all 3 of them on the updated "Baldwin, Phillips & Terlevich" (BPT; Baldwin et al. 1981) diagram of Trouille et al. (2011) shown in Figure 4. Galaxies A, B, and C are designated by orange, magenta, and red squares, while in the background we plot the density distribution of nearby ($0.02 < z < 0.35$) emission line galaxy ratios with S/N >5 from the SDSS spectroscopic data from Data Release 8 (DR8; Aihara et al. 2011). Comparison with other overplotted FRB hosts line ratios is made in Section 4.5.

From this, we see that B and C galaxies fall within the region where the optical emission line ratios are dominated by star formation, while A appears to have a nonnegligible contribution from an active galactic nucleus (AGN) to its optical line ratios. We note that there are no error bars associated with emission line fluxes for galaxies A and C (which were taken from LAMOST and SDSS, respectively; see above). From examining these archival spectra, we find that both H_α and [N II] are strongly detected while [O III] (and H_β in the case of galaxy A) fall in noisy regions of the spectra. However, if we assume a conservative error of 30% (corresponding to a 3σ detection of these lines), the resulting errors would not be significant enough to shift either galaxy from the star-forming or composite region of the BPT diagram, respectively. As a result, we consider these broad classifications robust and calculate other properties of star formation in the host galaxies (star formation rate, metallicity) for B and C only. We do not

Table 2
Summary of PRS Searches for the Host Galaxies of FRB 20200223B (A), FRB 20190110C (B) and FRB 20191106C (C)

Survey	Frequency	Angular	A Flux Density	B Flux Density	C Flux Density	References
	(MHz)	Resolution ($''$)	(mJy)	(mJy)	(mJy)	
FIRST	1400	5	<0.75[a]	<0.75[a]	<0.75[a]	Becker et al. (1995)
NVSS	1400	45	<12.5[a]	<12.5[a]	<12.5[a]	Condon et al. (1998)
VLASS	3000	2.5	<0.69[a]	<0.60[a]	<0.63[a]	Lacy et al. (2020)
TGSS ADR1	150	25	<17.5[a]	<17.5[a]	<17.5[a]	Intema et al. (2017)
LoTSS	144	6	2.96 ± 0.59	<0.42[a]	3.29 ± 0.14	Shimwell et al. 2022

Notes.
[a] 5σ rms sensitivity or upper limit.

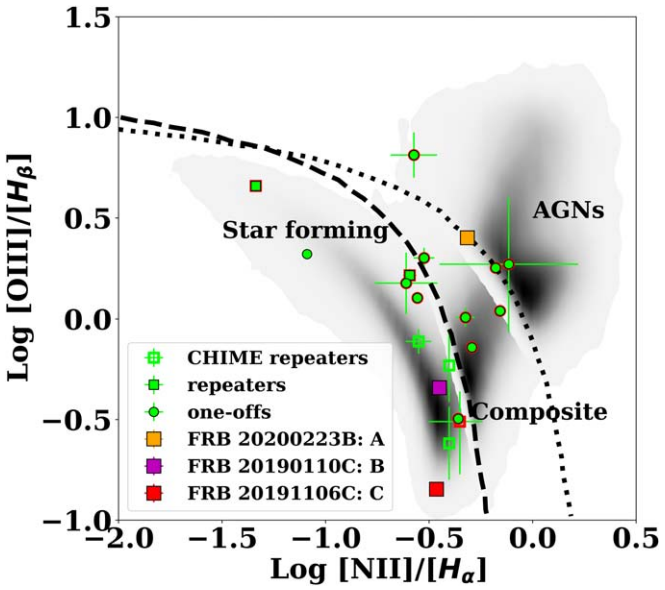

Figure 4. BPT diagram showing the dominant source of ionization using the nebular emission line ratios from the 3 plausible host galaxies and other previously published FRB hosts. The gray-scale background represents the density of galaxies from SDSS DR8 (Aihara et al. 2011). The dashed line (Kauffmann et al. 2003) indicates the empirical division between star-forming galaxies and AGNs while the dotted line (Kewley et al. 2001) shows the theoretical demarcation. FRB repeaters and one-offs are represented with squares and circles respectively while the ones with robust host associations ($\sim < 1''$) have red-edge color. The hollow green squares are other CHIME/FRB repeaters while the filled red, purple, and orange squares indicate the 3 host galaxies proposed here for CHIME/FRB repeaters. The location of the two galaxies (B and C) clearly suggests star formation while the location of A indicates an AGN contribution to the line fluxes. The representative repeating and nonrepeating FRBs' line ratios taken from Heintz et al. (2020), Bhardwaj et al. (2021b), Bhandari et al. (2022a), Fong et al. (2021), Mannings et al. (2021), and Michilli et al. (2023) indicates that most FRB host galaxies, especially repeaters, are mostly star-forming galaxies. See Section 4.5 for details.

calculate the star formation rate and metallicity for A due to the AGN contamination.

Star formation rates. In the absence of internal extinction as was evident from the Balmer decrement of each of the three galaxies, we calculate star formation rates from the H_α line fluxes for B and C without Balmer decrement correction using the equations from Kennicutt (1998): $\mathrm{SFR}(H_\alpha) = 7.9 \times 10^{-42}\ (L_{H_\alpha})$. From this, we find star formation rates of $0.1575(6) M_\odot\ \mathrm{yr}^{-1}$ at $L_{H_\alpha} = 1.994(7) \times 10^{40}\ \mathrm{erg\ s}^{-1}$ taken from the spectrum shown in Figure 3 for B, and $1.53\ M_\odot\ \mathrm{yr}^{-1}$ at $L_{H_\alpha} = 1.94 \times 10^{41}\ \mathrm{erg\ s}^{-1}$ for C (See Table 3). These values are consistent with galaxies with active star formation.

Metallicity. We calculate metallicities using Equation (1) from Pettini & Pagel (2004; $12 + \log(\mathrm{O/H}) = 8.90 + 0.57 \times \mathrm{N2}$), where $\mathrm{N2} = [\mathrm{N\,II}]\lambda 6583/\mathrm{H}_\alpha$. Using these ratios to estimate the metallicity of the galaxy resulted in an oxygen abundance of 9.102(2), which is equivalent to 2.76(1) $Z_\odot$ metallicity for B; and 9.10, which is equivalent to 2.7 $Z_\odot$ metallicity for C. These are high metallicities expected from an old population.

4.2. `Prospector` SED Fitting

We fitted the observed photometric data and spectroscopic redshifts using the stellar population synthesis modeling code `Prospector` (Johnson et al. 2021), in order to determine the stellar mass of galaxies A and B (the mass of galaxy C properties was previously published by Chang et al. 2015; hence, there was no need to carry out SED fitting for it). `Prospector` uses the stellar population synthesis library provided in the flexible stellar populations synthesis (FSPS) stellar population code `python-fsps` (Conroy et al. 2009) to fit the observed photometric data shown in Table 4. We assumed a Chabrier initial mass function Chabrier (2003) and allowed a delayed-τ star formation history (SFH) model (Carnall et al. 2019) that has 5 free parameters (stellar mass, stellar metallicity, galaxy age, dust attenuation optical depth for a foreground screen, and star formation timescale for an exponentially declining SFH). Reasonable priors as listed in Table 5 were set for the free parameters. The likelihood given the free parameters was then sampled using a Markov Chain Monte Carlo (MCMC) approach through the `emcee` code (Foreman-Mackey et al. 2013), and the posterior distributions were calculated. The extinction-corrected photometry was converted to flux densities as listed in Table 4.

The best-fit SED profiles of A (left panel) and B (right panel) are shown in Figure 5. Since we did not fit the spectra of galaxy B, we plot only the photometry and the fitted model. In Table 3, we present values for stellar mass, age, and SFR from our `Prospector` analysis of galaxies A and B along with values for stellar mass and SFR for galaxy C from (Chang et al. 2015). `Prospector` estimates SFR using the posteriors for the stellar mass, galaxy age, and decay timescale. Based on these results, we find that galaxies A, B, and C are all relatively massive with $M_{\mathrm{gal}} \approx 2\text{–}6 \times 10^{10}\ M_\odot$. For galaxies B and C, we combine these masses with SFRs estimated from the spectroscopic analysis described above to compute specific star formation rates (sSFR; see Table 3).

Table 3
Properties of the Plausible Host Galaxies of FRB 20200223B (A), FRB 20190110C (B), and FRB 20191106C (C)

Observed Property	A Values	B Values	C Values
R.A. (J2000)	$00^h33^m04\overset{s}{.}68$ (0.″015)	$16^h37^m16\overset{s}{.}43$ (0.″022)	$13^h18^m19\overset{s}{.}23$ (0.″01)
Decl. (J2000)	+28°49′52.″60 (0.″021)	+41°26′36.″30 (0.″024)	+42°59′58.″97 (0.″01)
Galaxy name	SDSS J003304.68+284952.6	SDSS 163716.43+412636.2	SDSS J131819.23+425958.9
Galactic longitude (l) and latitude (b)	118.08, −33.86	65.57, +42.09	105.68, +73.22
Apparent r-band mag (AB)	16.080 ± 0.001	18.009 ± 0.006	17.306 ± 0.003
$E(B-V)$ (mag)	0.0483(8)	0.0078(5)	0.0197(8)
spectroscopic redshift, z_{spec}	0.06024(2)	0.12244(6)	0.10775(1)
Luminosity distance (Mpc)	278.97(9)	591.2(3)	515.32(4)
Effective radius, R_{eff} (kpc)[e]	7.83 ± 0.03	9.65 ± 0.09	4.01 ± 0.01
M_r	−21.15 ± 0.01	−20.71 ± 0.02	−21.20 ± 0.01
$M_u - M_r$	1.84 ± 0.05	1.64 ± 0.11	2.08 ± 0.07
H_α	8.63×10^{-15}[f]	$4.8042(8)\times10^{-16}$	6.09×10^{-15}[f]
H_β	1.17×10^{-15}[f]	$6.43(8)\times10^{-17}$	8.88×10^{-16}[f]
[O III](λ5006 Å)	2.94×10^{-15}[f]	$2.93(7)\times10^{-17}$	1.27×10^{-16}[f]
[N II](λ6582 Å)	4.17×10^{-15}[f]	$1.703(9)\times10^{-16}$	2.09×10^{-15}[f]
Inferred Property			
SFR_{H_α} ($M_\odot$ yr^{-1})[a]	N/A	0.1575(6)	1.53[f]
Oxygen abundance [Log_{10} (O/H)][a] + 12	N/A	9.102(2)	9.10[f]
SFR ($M_\odot$ yr^{-1})[b]	$0.59^{+0.04}_{-0.04}$	$0.54^{+0.04}_{-0.04}$	$4.75^{+1.29}_{-1.27}$[c]
Stellar mass ($M_\odot$)[b]	$5.6^{+1.14}_{-0.93}\times10^{10}$	$2.5^{+0.10}_{-0.17}\times10^{10}$	$4.5^{+1.2}_{-1.2}\times10^{10}$[c]
Mass weighted age (Gyr)[b]	$3.37^{+0.47}_{-0.73}$	$2.59^{+0.80}_{-1.24}$	-
Specific star formation rate [log(sSFR)] (yr^{-1})	$-10.98^{+0.00}_{-0.03}$[d]	$-10.66^{+0.07}_{-0.14}$[d]	$-10.61^{+0.14}_{-0.21}$[c]

Notes. N/A represents parameter estimates that are not reliable, and hence not published.
[a] Values obtained using the optical spectrum of the host galaxies.
[b] Value estimated from `Prospector`.
[c] Published values obtained from literature (Chang et al. 2015).
[d] Values obtained using SFR and the stellar mass values from the `Prospector` analysis.
[e] Values are half-light radius taken from DESI legacy catalog (Dey et al. 2019).
[f] Values published without errors. Our analysis of these data shows that the errors will not change the result of our analysis.

Table 4
Photometric Data Used for `Prospector` SED Fitting for Galaxies, A and B

Data Set	Filter	Central Wavelength (Å)	A Flux Density	B Flux Density
GALEX	FUV	1528	1.68×10^{-8}	4.85×10^{-9}
	NUV	2271	2.23×10^{-8}	6.98×10^{-9}
SDSS	u	3543	6.83×10^{-8}	1.23×10^{-8}
	g	4770	2.18×10^{-7}	3.49×10^{-8}
	r	6231	3.72×10^{-7}	5.54×10^{-8}
	i	7625	4.95×10^{-7}	7.43×10^{-8}
	z	9134	6.38×10^{-7}	7.91×10^{-8}
2MASS	J	12,350	9.28×10^{-7}	⋯
	K	16,620	5.95×10^{-7}	⋯
	Ks	21,590	7.58×10^{-7}	⋯
WISE	W1	33,526	2.19×10^{-7}	4.32×10^{-8}
	W2	46,028	1.49×10^{-7}	2.79×10^{-8}
Spitzer[a]	3.6 μm	35,510	⋯	2.71×10^{-8}
	4.5 μm	44,930	⋯	1.98×10^{-8}
	5.8 μm	57,300	⋯	1.86×10^{-8}
	8.0 μm	78,730	⋯	1.24×10^{-8}

Notes. All flux densities are in maggies. Near-UV (NUV). Far-UV (FUV).
[a] Flux densities are for 3.″8 diameter aperture.

4.3. Constraints on the Presence of Persistent Radio Sources

In the field of FRB 20200223B, we found a source in the high-resolution LoTSS (Shimwell et al. 2022) LoTSS catalog, ILT J003304.67+284952.4 with an integrated flux density of 2.96 ± 0.59 mJy and an isotropic radio luminosity of $2.7(5)\times10^{29}$ erg s^{-1} Hz^{-1} at 144 MHz given the luminosity distance of 277.81 Mpc. The radio source is resolved and extended in the LoTSS, with an FWHM of the major axis width of 19.53" (LoTSS beam size, $\theta = 6''$) and also spatially coincident with galaxy A. The radio contours match the optical morphology implying that the radio emission originates from star formation activity from the galaxy (see the left panel of Figure 1). We used the VLASS upper limit of <0.69 mJy (5σ) at 3 GHz and the LoTSS detection at 144 MHz to estimate an upper limit on the spectral index ($S_\nu \approx \nu^\alpha$) of the radio source as $\alpha_{radio} < -0.48 \pm 0.09$, which is consistent with star formation in the galaxy. Also, the radio-to-optical flux ratio of < 0.4 is consistent with the star formation as opposed to AGN activity (radio-to-optical flux ratio, $F_{1.4\,GHz}/F_{r-mag} > 1.4$; e.g., Machalski & Condon 1999; Vega et al. 2008; Padovani et al. 2009). Therefore, we conclude that the radio source is likely a low-frequency emission coming from star formation in the host galaxy. Due to the large beam size, $\theta = 6''$ of LoTSS, we cannot rule out a faint PRS embedded in this emission.

In the field of FRB 20190110C, we found unresolved radio sources in FIRST (FIRST J163717.8+412634), VLASS (VLASS 1QLCIR J163717.83+412633.9: Epochs 1 and 2), and LoTSS (ILT J163717.72+412633.8) catalogs in the field spatially coincident with one another but not with the plausible host galaxy, B. There is no source found in NVSS down to a 5σ threshold of 12.5 mJy beam^{-1}. The integrated radio flux

Table 5
Priors Used for `Prospector` SED Fitting for Galaxies, A and B

Prior Description			A	B
Total stellar mass formed	$\log(M_*/M_\odot)$	log-uniform	min = 9, max = 11	min = 9, max = 12
Stellar metallicity	$\log(Z/Z_\odot)$	top-hat	min = −2, max = 1	min = −5, max = 1
Diffuse V-band dust optical depth	dust2	top-hat	min = 0, max = 0.3	min = 0, max = 5
Stellar population age of the galaxy	t_{age} (Gyr)	log-uniform	min = 5, max = 12	min = 1, max = 10
E-folding time of the SFH	τ (Gyr)	log-uniform	min = 0.05, max = 10	min = 0.05, max = 10

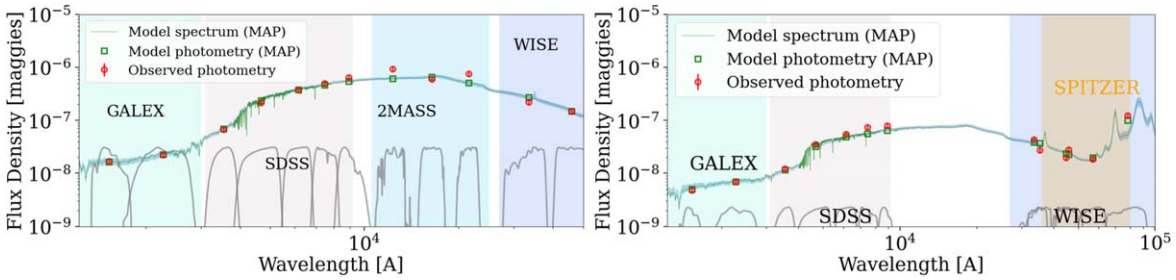

Figure 5. Left: best-fit `Prospector` model spectrum for A, the plausible host of FRB 20200223B, plotted along with the flux density in different wavelength bands. Right: Best-fit `Prospector` model spectrum for B, the plausible host of FRB 20190110C. Different wavelength broadband filters are represented in different colors from ultraviolet to infrared from GALEX, SDSS, 2MASS, SPITZER, and WISE catalogs. The best-fit model spectra are used to estimate different physical properties for A and B, as summarized in Table 3.

density for the FIRST source is 0.91 ± 0.15 mJy; for the first epoch of VLASS is 0.85 ± 0.11 mJy; for the second epoch of VLASS is 0.72 ± 0.11 mJy; and for the LoTSS source is 8.67 ± 0.14 mJy. The detailed analysis of this radio source will be published by A. L. Ibik et al. (2023, in preparation). We report the measured upper limits from the B location in Table 2.

In the field of FRB 20191106C, we found five LoTSS sources with one (ILT J131819.22+425958.9, shown in the right panel of Figure 1) spatially coincident with the plausible host galaxy, C. For simplicity, we show only the radio source contours that are spatially coincident with the plausible host galaxy. This source, ILT J131819.22+425958.9, has an integrated flux density of 3.29 ± 0.14 mJy and a radio luminosity of $1.05 \pm 0.04 \times 10^{30}$ erg s^{-1} Hz^{-1} at 144 MHz given the luminosity distance of 516.60 Mpc. The radio source is slightly resolved in the LoTSS, with an FWHM major axis width of $7\farcs76$, and is offset by 4.0 ± 1.2 kpc from the center of the host galaxy. We used the VLASS upper limit of <0.63 mJy (5σ) at 3 GHz and the LoTSS detection at 144 MHz to estimate a spectral index $\alpha_{radio} < -0.54 \pm 0.02$. The spectral index and the radio-to-optical ratio of < 0.9 are both consistent with star formation as opposed to AGN activity. Therefore, we conclude that the radio source is likely a low-frequency emission coming from star formation in the host galaxy. Due to the large beam size, $\theta = 6''$ of LoTSS, we cannot rule out a faint PRS if embedded in the emission.

4.4. Estimates of Host Dispersion Measures

To characterize DM_{host} of a galaxy, we first need to properly assess any additional foreground contributions to the DM from intervening structures. Typically, using the equation DM_{host}=$DM_{observed}$ − DM_{MW}(NE2001) − DM_{halo} − DM_{IGM}, any missed or unaccounted intervening media will reduce the estimated value of DM_{host}. We searched within our FRB baseband positions for foreground galaxy clusters using data from Wen et al. (2009, 2012, 2018), Wen & Han (2015), and Banerjee et al. (2018); Galactic H II-regions using the H_α maps from Anderson et al. (2014), Green (2019); Galactic star-forming regions using CO maps from Avedisova (2002), Rice et al. (2016); nearby galaxies from GLADE v2.3 (Dálya et al. 2018); and dwarf galaxies from McConnachie (2012).

The results show that there are no star-forming or H II-regions in the foreground of the searched FRB repeaters in our sample listed in Table 1. We will now estimate DM_{host} for the 3 FRBs with plausible hosts discussed in this work and discuss the result of the few cases where there is at least one galaxy cluster or a galaxy in the region.

For the case of FRB 20200223B, in the absence of any object along the line of sight of the plausible host, we use $z_{spec} = 0.06024(2)$, to obtain $DM_{IGM} = 57.12(2)$ pc cm^{-3} following Equation (2) of Macquart et al. (2020). We chose a range of DM_{halo} with the lower bound and a higher bound that will produce a physical DM_{host} for each FRB but still within the given range reported by Dolag et al. (2015), Yamasaki & Totani (2020), and Cook et al. (2023), which is 30–98 pc cm^{-3} for this FRB. Taking note of the DM_{MW}(NE2001) = 45(9) pc cm^{-3}, we estimate DM_{host} = 1–73 pc cm^{-3}.

We do not find any object along the line of sight of the host galaxy of FRB 20190110C. We, therefore, use $z_{spec} = 0.12244(6)$ for the host galaxy to directly estimate DM_{IGM} and hence DM_{host}. For DM_{MW}(NE2001) = 37(7) pc cm^{-3}, and assuming DM_{halo} = 30–65 pc cm^{-3}, we obtain $DM_{IGM} = 117.75(6)$ pc cm^{-3}, and DM_{host} = 2 –33 pc cm^{-3}.

In the field of FRB 20191106C, there is a galaxy cluster, WHL J131827.1+425803 (Wen & Han 2015), with $z_{spec} = 0.47$. Given $z_{max} = 0.36$, we do not expect that the galaxy cluster will affect the DM of the FRB. There are many other galaxies in the field, but none of them has a redshift that could contribute to the DM of the FRB. In the absence of any intervening medium, we estimate DM_{host} = 103–187 pc cm^{-3}, from $DM_{IGM} = 103.29(1)$ pc cm^{-3}, at $z_{spec} = 0.10775(1)$ of the host galaxy, assuming DM_{halo} = 30–111 pc cm^{-3}, and DM_{MW}(NE2001) = 25(5) pc cm^{-3}.

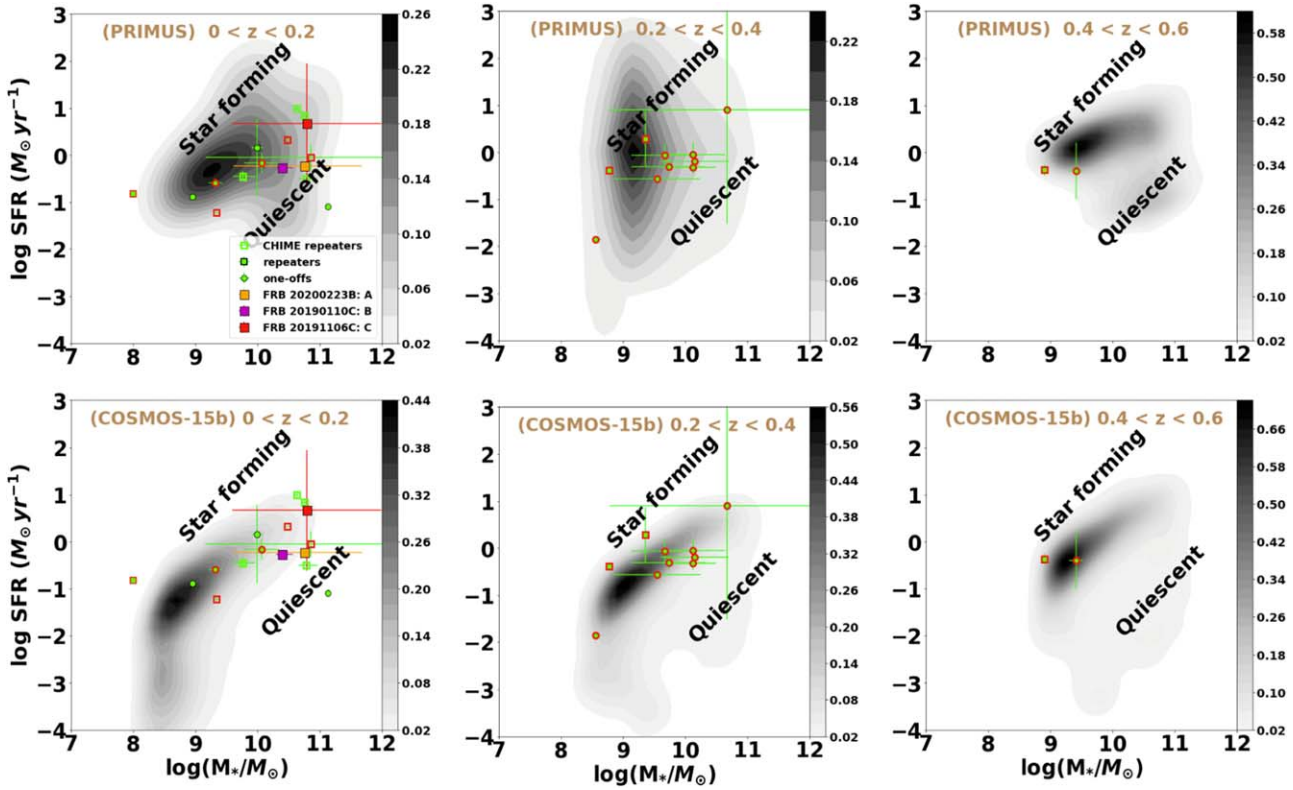

Figure 6. Star formation rate vs. stellar mass distribution of FRB hosts in three redshift ranges. The squares and circles in each plot represent repeating and one-off FRBs respectively (Mahony et al. 2018; Heintz et al. 2020; Bhardwaj et al. 2021a; Bhandari et al. 2022a, 2023; Bhardwaj et al. 2021b; Fong et al. 2021; Mannings et al. 2021; Niu et al. 2022; Michilli et al. 2023; Sharma et al. 2023) while the ones with robust host associations ($\sim < 1''$) have red-edge color. The hollow green squares are other CHIME/FRB repeaters while the filled red, purple, and orange squares indicate the 3 host galaxies proposed here for CHIME/FRB repeaters. The gray background is a kernel density distribution of the PRIMUS survey galaxy sample for the top panel and COSMOS-15b for the bottom panel. While the hosts of repeating FRBs show diverse SFR behavior, only a few FRBs are associated with transitioning and quiescent galaxies. Most FRB hosts are slightly offset below the star-forming main sequence when compared to the PRIMUS data set in the redshift range $0 < z < 0.2$. While this effect is less strong compared to COSMIS-15b data, in each case, a subset of FRB-repeater hosts (including those presented here) still exhibit low star formation for their galaxy mass. We discuss this issue further in Section 4.5.

For the rest of this section, we take note of any possible intervening structures for the other 10 repeaters in our sample, for which we do not yet have host associations, but for which one should beware if host galaxy associations are made in the future. We found a nearby galaxy cluster (WHL J172540.4 +550250; Wen et al. 2009) with redshift $z = 0.43$ in the field of FRB 20190804E. However, we do not think that this galaxy cluster could affect the DM of the FRB as it has $z_{\rm max} = 0.37$. In the field of FRB 20201114A with $z_{\rm max} = 0.33$, we found a GLADE galaxy (HyperLEDA catalog number: 2745781) with $z_{\rm spec} = 0.08$ (Dálya et al. 2018) and 4 other galaxies from the DESI catalog, all having $z < z_{\rm max}$.

We also found 4 galaxy clusters, namely WHL J010806.9 +182752 ($z_{\rm spec} = 0.17$), WHL J010830.7+183100 ($z_{\rm spec} = 0.56$), WHL J010833.0+182514 ($z_{\rm spec} = 0.46$; Wen & Han 2015), and AMF9 J010830.7+182754 ($z_{\rm spec} = 0.19$; Banerjee et al. 2018) in the field of FRB 20200929C. Since their redshifts are lower compared to the FRB's $z_{\rm max} = 0.44$, it is plausible that WHL J010806.9+182752 and AMF9 J010830.7+182754 could affect the DM of the FRB depending on the location and redshift of the host galaxy.

4.5. Comparison to Previous FRB Hosts

Based on the results found above, the three probable FRB host galaxies presented here are all relatively massive galaxies with signatures of ongoing star formation and roughly solar metallicity. Here, we compare these properties to those of other known FRB hosts. To aid this comparison, we plot galaxies A, B, and C along with other FRB hosts on a BPT diagram (Figure 4), a mass–star formation rate diagram (Figure 6), a color–magnitude diagram (Figure 7) and a mass–metallicity diagram (Figure 8). In all plots, FRB hosts from the literature are shown in green, with repeaters designated as squares and one-offs as circles. Previous repeating FRBs that were identified by CHIME/FRB are shown as open squares. FRBs with robust host association are shown as red-edge-colored markers.

BPT diagram. First, to compare the dominant sources of photoionization in FRBs host galaxies, we add FRBs from the literature to the BPT diagram described in Section 4.1 to get Figure 4. A total of 15 FRB hosts emission line fluxes were taken from Heintz et al. (2020), Bhardwaj et al. (2021b), Bhandari et al. (2022a), Fong et al. (2021), Mannings et al. (2021), and Michilli et al. (2023) and shown in green squares and circles for 5 repeating (the hosts of FRB 20190303A are two merging galaxies, which leads to 6 open squares in the figure) and 10 nonrepeating FRBs. Out of the 15 FRBs, 3 repeaters and 9 one-offs have robust (FRBs with localization region of $\sim < 1''$) host associations (see markers with red-edge colors in Figure 4). The plot shows that the 3 host galaxies (A, B, C) line ratios are broadly consistent with those of most

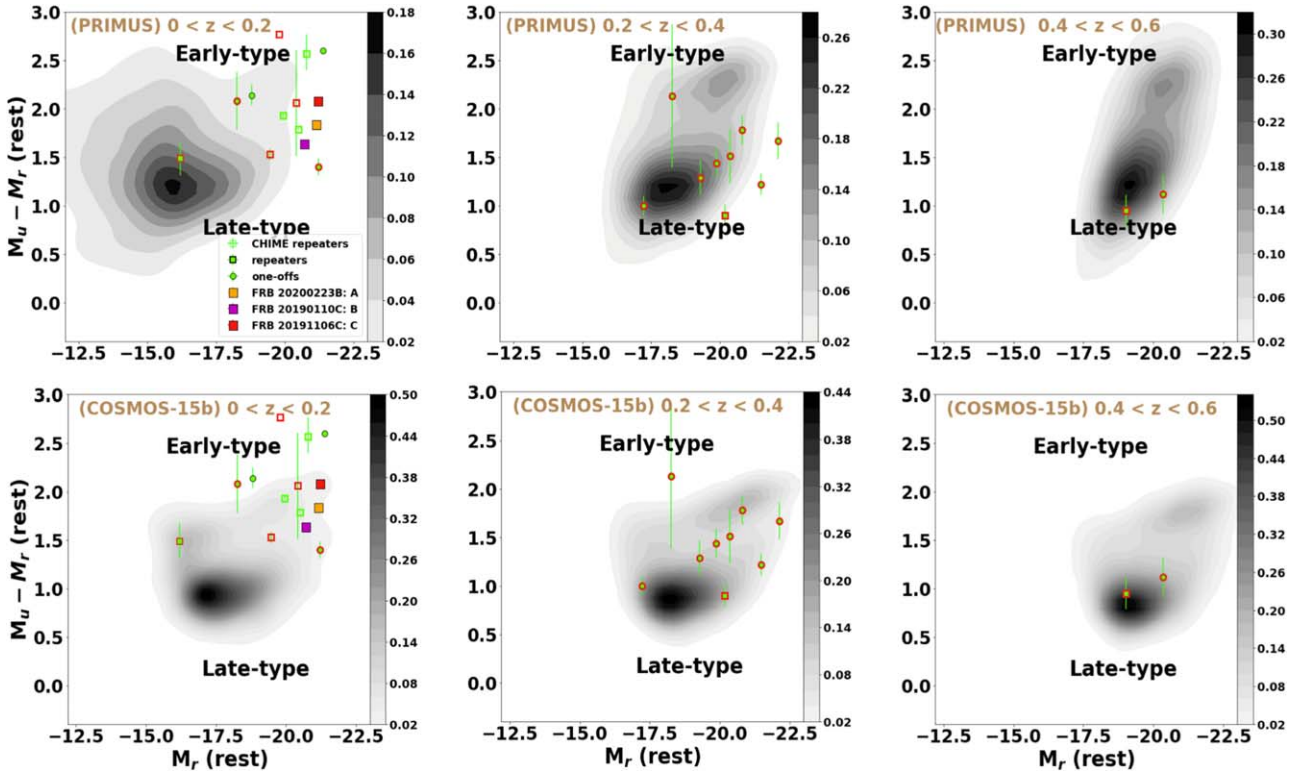

Figure 7. Rest-frame color–magnitude diagram in three redshift ranges showing a gray background of the galaxy population from the PRIMUS survey (Moustakas et al. 2013) for the top panel and the field galaxies from the COSMOS-15 survey (Leja et al. 2020) for the bottom panel. The squares and circles in each plot represent repeating and one-off FRBs respectively (Mahony et al. 2018; Heintz et al. 2020; Bhardwaj et al. 2021a; Bhandari et al. 2022a, 2023; Bhardwaj et al. 2021b; Fong et al. 2021; Mannings et al. 2021; Michilli et al. 2023; Sharma et al. 2023) while the ones with robust host associations ($\sim < 1''$) have red-edge color. The hollow green squares are other CHIME/FRB repeaters while the filled red, purple, and orange squares indicate the 3 host galaxies proposed here for CHIME/FRB repeaters. Many FRBs come from bright galaxies, and there is a diversity of early-type, late-type, and *green-valley* (parameter space between the two peaks—early-type and late-type) galaxies among repeaters and one-offs. Approximately half of the FRB-repeater hosts show evidence of being in the transitional green-valley and early-type irrespective of data sets. See Section 4.5 for details.

FRB hosts, although galaxy A would be the first host for a *repeating* FRB with signatures of AGN activity. Galaxies B and C support the trend identified by Bhandari et al. (2022a) that most repeating FRBs happen in galaxies where star formation is the dominant source of photoionization, thus disfavoring progenitor channels where AGN activity is required (e.g., Katz 2017; Vieyro et al. 2017; Gupta & Saini 2018).

SFR–Mass. In Figure 6, we compare the rate of star formation versus the stellar mass of FRB host galaxies in three redshift bins, $0 < z < 0.2$, $0.2 < z < 0.4$, and $0.4 < z < 0.6$. SFRs, and the masses for 24 FRB hosts were extracted from Mahony et al. (2018), Heintz et al. (2020), Bhardwaj et al. (2021a), Bhandari et al. (2022a, 2023), Fong et al. (2021), Mannings et al. (2021), Bhardwaj et al. (2021b), Niu et al. (2022), Michilli et al. (2023), and Sharma et al. (2023) and shown in green squares and circles for 10 repeating (the hosts of FRB 20190303A are two merging galaxies, which leads to 11 open squares in the figure) and 14 nonrepeating FRBs. Out of the 24 FRBs, 7 repeaters and 11 one-offs have robust (FRBs with localization region of $\sim < 1''$) host associations (see markers with red-edge colors in Figure 6). We plot the location of galaxies A, B, and C using SFRs, and stellar masses measured from `Prospector` SED fitting described above.

In the top left panel, the kernel density contours represent galaxies from the PRism MUlti-object Survey (PRIMUS) survey (Moustakas et al. 2013) with redshifts $z < 0.5$. In the bottom left panel, the kernel density contours represent galaxies from the COSMOS-15 sample that were modeled by Leja et al. (2020), referred to as COSMOS-15b. Bhandari et al. (2022a) previously identified that most FRB host galaxies are offset slightly below the star-forming main sequence, showing low star formation rates for their masses when compared to the PRIMUS data set. This offset is visible in our figure (see Figure 6), where the star-forming main sequence is shifted about half an order of magnitude lower in the upper panels (PRIMUS) of Figure 6. In agreement with the result of Gordon et al. (2023), when compared to the lower panel (COSMOS15b), the galaxies mostly fall within the star-forming main sequence in closer alignment to many of the known FRB hosts. While reconciling this discrepancy is beyond the scope of this work, we note the following: (i) Our data sets are a mix of both spectroscopic measurements and SED-derived information, and so some are model-dependent. This makes it difficult to select direct analogous survey data for comparison; (ii) we note that, below redshift < 0.2, the PRIMUS sample has fewer galaxies compared to higher redshift field galaxies and lacks quality SFR and stellar mass measurements within this redshift range; (iii) the PRIMUS data set redshifts are however measured from spectroscopy, and the

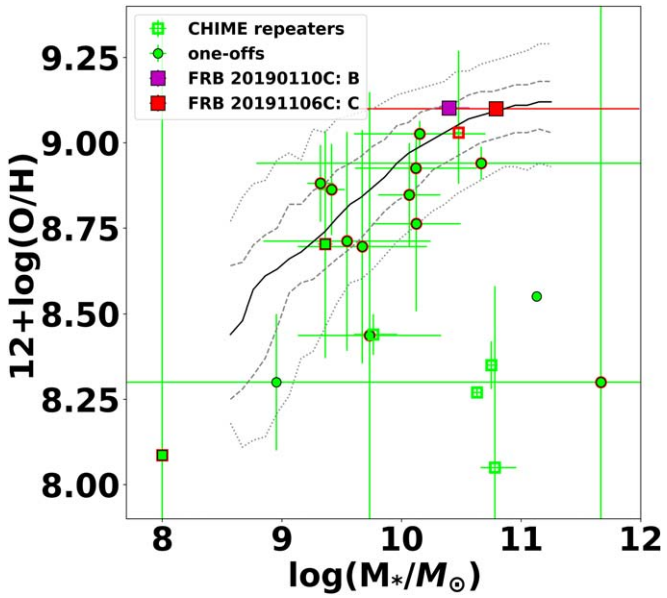

Figure 8. A plot of metallicity vs. the stellar mass of galaxies. FRB repeaters and one-offs are represented with squares and circles respectively (Heintz et al. 2020; Bhandari et al. 2022a; Bhardwaj et al. 2021b; Mannings et al. 2021; Michilli et al. 2023; Sharma et al. 2023) while the ones with robust host associations ($\sim < 1''$) have red-edge color. The hollow green squares are other CHIME/FRB repeaters while the filled red and purple squares indicate 2 out of the 3 host galaxies proposed here for CHIME/FRB repeaters. The third galaxy, A, was not included in this plot since the nebular emission is contaminated by AGN activity. The solid black line is the median of the SDSS metallicity–stellar mass distribution, and the gray dashed and dotted lines cover the 68% and 95% confidence regions (Tremonti et al. 2004). Overall, there is no metallicity preference between repeaters and one-offs, but most of them are slightly below the solid line. See Section 4.5 for details.

derived galaxy property values are from parameterized SFH; (iv) the COSMOS-15b data set on the other hand has redshift measurements from a mixture of spectroscopic and photometric data while its galaxy properties are derived values from a nonparametric continuity SFH.

Compared to *both* comparison data sets, galaxies A, B, and C (and many of the other CHIME repeaters) lie along and below the star-forming main sequence. In addition, the WISE plot location of galaxy A, showing ongoing star formation coupled with emission line signatures showing AGN activity, is also consistent with a galaxy in a transition phase. Our findings show that most FRBs appear to come from star-forming galaxies across the FRB redshift range observed so far. While the hosts of repeating FRBs show diverse SFR behavior, only a few FRBs are associated with transitioning and quiescent galaxies. Most FRB hosts are slightly offset below the star-forming main sequence when compared to the PRIMUS data set in the redshift range $0 < z < 0.2$. While this effect is less strong compared to the COSMOS-15b data, in each case, a subset of FRB-repeater hosts (including those presented here) still exhibit a low star formation for their galaxy mass.

Overall, even though most FRB hosts prefer star-forming hosts, there may be an observational bias against finding FRBs in star-forming regions due to large possible levels of pulse dispersion and scattering in such regions. This could lead to decreased sensitivity to repeating bursts (Gordon et al. 2023). The difference in the SED-modeling methods used for the two field galaxy data sets and the insufficient data for a given redshift range are possible factors that could affect the interpretation of this result.

Gordon et al. (2023) also used the mass-doubling number criterion (the number of times the stellar mass doubles within the age of the universe at redshift at the redshift of the galaxy assuming a constant sSFR) described by Tacchella et al. (2022) to classify galaxies as star-forming, transitioning, and quiescent. We adopted this method for all the galaxies in our comparison sample as well as galaxies A, B, and C (even though we caution that the criterion was developed for galaxy properties derived using nonparametric star formation histories). Our results of the literature comparison sample show that most FRB hosts are star-forming, few are transitioning, and one is quiescent. In addition, galaxies A and B are both transitioning while C is star-forming according to the criteria with mass-doubling numbers of 0.1363, 0.2686, and 0.9547 respectively. Together, we note that all four galaxies classified as transitioning by this metric were repeaters. The overall outcome (that many FRB hosts are star-forming) is however consistent with the conclusions of Gordon et al. (2023), Sharma et al. (2023).

Color–Magnitude. To further examine the possibility that a subset of repeating FRB hosts are in a transitional phase, in Figure 7, we compare the color–magnitude properties of the FRB hosts in three redshift bins, $0 < z < 0.2$, $0.2 < z < 0.4$, and $0.4 < z < 0.6$. This can be a useful indicator of the class of stellar population in the galaxies, which is less model-dependent. Specifically, the plot of the rest-frame $M_u - M_r$ colors versus their absolute r-band magnitudes, M_r, is overplotted with the kernel density contours of field galaxies. The top panel again compares to galaxies from the PRIMUS survey with redshifts $z < 0.5$, and the lower panel compares with galaxies of the COSMOS-15b (Leja et al. 2020) data set retrieved from the parent catalog (Laigle et al. 2016). A total of 21 FRB hosts' color–magnitude values were extracted from Mahony et al. (2018), Heintz et al. (2020), Bhandari et al. (2022a, 2023), Bhardwaj et al. (2021a, 2021b), Fong et al. (2021), Mannings et al. (2021), Michilli et al. (2023), and Sharma et al. (2023) and shown in green squares and circles for 8 repeating (the hosts of FRB 20190303A are two merging galaxies which leads to 9 open squares in the figure) and 13 nonrepeating FRBs. Out of the 21 FRBs, 6 repeaters and 11 one-offs have robust (FRBs with localization region of $\sim < 1''$) host associations (see markers with red-edge colors in Figure 7). Galaxies A, B, and C are bright but fall within the overall range of properties seen in the literature for the FRB hosts. Many FRBs come from bright galaxies, and there is a diversity of early-type, late-type, and *green-valley* (parameter space between the two peaks—early-type and late-type) galaxies among repeaters and one-offs.

Our result shows that the observed colors for all three probable hosts presented in this manuscript fall within the *green valley* when compared to the PRIMUS data set, which would be consistent with having low star formation rates for their stellar masses (we note that the PRIMUS data set has very few quiescent galaxies in the redshift range $0 < z < 0.2$, which is why there is no corresponding *early-type* island in the left top panel). In particular, with the addition of these hosts, *half* of the FRB repeaters shown in Figure 7 have colors between $1.6\,\mathrm{mag} < M_u - M_r < 2.1\,\mathrm{mag}$.

When comparing to the COSMOS-15b data set, we again see that the three probable hosts described here show redder colors

than a majority of late-time galaxies. (We note that the Leja et al. 2020 sample has very few quiescent galaxies, which is why there is a small corresponding "early-type" islands in all the lower panels.) We note that this is a slightly different behavior that was observed with the SFR–stellar mass plot for the COSMOS-15b data set (lower panels Figure 6) where many FRBs fell directly on the SFR main sequence. Given that the exact same set of galaxies are plotted in both figures, this distinction must stem from methods used to measure the star formation rate and stellar mass for the COSMOS-15b and FRB data sets (see above).

Approximately half of the FRB-repeater hosts show evidence of being in the transitional green-valley and early-type, irrespective of data sets. The moderate and low SFR seen for most FRB hosts are consistent with the location on the color–magnitude diagram. Most of the hosts are in the green valley and have a redder color possibly because of their low current star formation. This result is however nonintuitive as previous analysis shows that FRB hosts are mostly star-forming (which is mostly associated with late-type galaxies). It is possible that many FRBs are coming from star-forming regions of either late-type or green-valley galaxies. Indeed, we see evidence above for ongoing star formation within the potential FRB hosts presented here. Alternatively, this may be evidence for an additional, older, FRB progenitor channel, which is slightly overrepresented in the repeater population. Indeed, there has been recent evidence for some FRBs coming from older environments, such as FRB 20200120E found in a globular cluster of a spiral galaxy (Bhardwaj et al. 2021a; Kirsten et al. 2022). Finally, it is possible that this outcome is a selection bias since it may be easier to see FRBs from early-type galaxies given that they are not obscured by a high degree of dispersion and scattering from ionized gas in the hosts (Mannings et al. 2021).

Mass–Metallicity. Finally, Figure 8 shows the distribution of host galaxies' metallicities and stellar masses. These are shown in comparison to the Tremonti et al. (2004) stellar mass versus gas-phase metallicity relationship found from SDSS data of redshifts $z \sim 0.1$. The solid black line is the median, and the gray dashed and dotted lines cover the 68% and 95% confidence regions. Host information for 19 other FRBs was extracted from Heintz et al. (2020), Bhardwaj et al. (2021b), Bhandari et al. (2022a), Mannings et al. (2021), Michilli et al. (2023), and Sharma et al. (2023) consisting of 6 repeaters (the hosts of FRB 20190303A are two merging galaxies, which leads to 7 open squares in the figure) and 13 one-offs. Out of the 19 FRBs, 3 repeaters and 11 one-offs have robust (FRBs with localization region of $\sim < 1''$) host associations (see markers with red-edge colors in Figure 8). In most cases, we extract raw emission line fluxes and calculate metallicity ourselves using the O3N2 calibration (Hirschauer et al. 2018). In 3 cases where the line fluxes were not available and we could not identify the metallicity calibration used, we took published metallicities directly, acknowledging that a small error may be present in their location within Figure 8 due to systematic offsets between the various strong line metallicity diagnostics (Kewley & Ellison 2008). Galaxies B and C are both relatively high-mass galaxies that fall directly on the mass–metallicity relationship of Tremonti et al. (2004). Overall, there is no metallicity preference between repeaters and one-offs, but most of them are slightly below the solid line. This supports the conclusion that FRBs, as a whole, do not require the low metallicity, high sSFR environments preferred by superluminous supernovae and long-duration gamma-ray bursts (Lunnan et al. 2014).

Trends with FRB repeat rate. We used the repeat rates reported by CHIME/FRB Collaboration & Andersen (2023) for 8 CHIME/FRB events in our sample to compare with host properties (metallicity, SFR, color). Out of these, 7 of them are clustered at similar low repeat rates ($<1\,\mathrm{hr}^{-1}$) with only one having a high repeat rate ($>1\,\mathrm{hr}^{-1}$). The results show no relationship between repeat rates and any of the properties given the current data. However, this is a very small data set; a larger sample collected in the future could provide more insight.

Trends with FRB $DM_{\rm host}$. We retrieved the FRB $\mathrm{DM_{host}}$ values of 24 FRBs containing 8 repeaters and 16 one-offs from Law et al. (2022). We included the $\mathrm{DM_{host}}$ estimates from FRB 20200223B, FRB 20190110C, and FRB 20191106C thereby increasing the sample of repeaters to 11 events. We applied the two-sample Kolmogorov–Smirnov test to the $\mathrm{DM_{host}}$ histogram distribution for repeaters and nonrepeaters. The result is a p-value of 0.4113 (∼41%). Assuming a null hypothesis at a 95% confidence interval that the repeaters and nonrepeaters have the same local environment, then a p-value that is less than 0.05 (5%) will reject the null hypothesis. In this case, the p-value is greater than 5%, thus in agreement with the null hypothesis stating that the two distributions are the same. We note that FRB 20190520B still has the highest $\mathrm{DM_{host}}$ in our limited sample despite its new reduced value (430^{+140}_{-220} $\mathrm{pc\,cm^{-3}}$) following the discovery of 2 galaxy clusters along its line of sight (Lee et al. 2023). However, repeating the test with the new value for FRB 20190520B does not change the conclusion.

In summary, the sample of about 24 known FRB of host galaxies (repeating and nonrepeating; Heintz et al. 2020; Bhandari et al. 2022a, 2023; Niu et al. 2022; Michilli et al. 2023) covers a broad range of r-band absolute magnitude, $M_u - M_r$ colors, stellar masses, star formation rates, and metallicities. The three new probable hosts identified here are consistent with this broader population. However, it is notable that, through a combination of intermediate $M_u - M_r$ colors (galaxies A, B, C), low star formation rate for a given stellar mass (galaxies A, B, C), mass-doubling timescale (galaxies A, B, C), or an elliptical morphology with signatures of ongoing star formation (galaxy C), all three show some evidence of being in a transitional or star-forming regime. Coupled with the previously published hosts, there is tentative evidence that FRB repeaters, in particular, are overrepresented in the star-forming and *green valley* with many showing $M_u - M_r$ colors redder than the majority of star-forming galaxies.

5. Summary

We searched for host galaxy associations for 13 FRB repeaters out of the 25 "gold" and 14 "silver" samples recently published by CHIME/FRB Collaboration & Andersen (2023). The CHIME/FRB baseband localization regions were searched for host galaxies in SDSS and DESI. We considered two methods to assess the probability of host association for candidate galaxies within the field. First, we run candidate host galaxies through `PATH` to estimate their probabilities of association with an FRB. Second, we consider the probability that a galaxy as bright as the host preferred by PATH would be found within the CHIME localization region by chance. When we consider the *look-elsewhere* effects associated with the fact

that we searched 13 CHIME/FRB localization regions, we do not find evidence for a significant overabundance of bright galaxies. However, under the assumption that FRBs come from galaxies, the Bayesian approach of PATH still allows us to consider the most probable host for an individual FRB.

In the end, we consider two FRBs (FRB 20200223B, FRB 20190110C) for which we have galaxy candidates with a maximum association probability that is greater than 90%. We also cautiously discuss a third FRB (FRB 20191106C) with a plausible host galaxy for which the archival surveys have a shallower depth at the maximum redshift of the FRB. We obtained a Max $P_{\rm PATH} = 81.5\%$, at $P(U) = 0.1$, but this galaxy was strongly preferred over any other galaxy in the field. The resulting discussed host galaxies for the 3 FRBs (FRB 20200223B, FRB 20190110C, and FRB 20191106C) are SDSS J003304.68+284952.6, SDSS 163716.43 +412636.2, and SDSS J131819.23+425958.9, respectively.

FRB 20200223B is likely located in a spiral, star-forming galaxy with evidence for AGN activity. FRB 20190110C likely comes from a high metallicity, irregular galaxy showing evidence of quenching star formation, while the potential host galaxy of FRB 20191106C is a high metallicity, possibly elliptical with evidence for ongoing star formation. The latter two galaxies follow the standard mass–metallicity relationship observed for nearby galaxies. Moreover, all 3 galaxies are in the transitional phase with regard to star formation and show redder colors than expected for late-type galaxies. This is consistent with the broader repeater host population, which appears to prefer the region between early- and late-type galaxies as discussed in Section 4.5. In addition, the high metallicity and low sSFR obtained for these galaxies are different from what is seen for the hosts of superluminous supernovae and long-duration gamma-ray bursts. However, it is critical to both confirm these host galaxies via arcsecond localization and to continue to increase the number of FRBs with robust host associations, since probabilistic host identification methods are biased toward bright galaxies.

Acknowledgments

We thank Kasper Heintz and Joel Leja for the supplementary information and code that facilitated this work. We sincerely appreciate Prof. Edward Wright and Chao-Wei Tsai for granting permission to use the WISE diagnostic plot from their paper.

We acknowledge that CHIME is located on the traditional, ancestral, and unceded territory of the Syilx/Okanagan people. We are grateful to the staff of the Dominion Radio Astrophysical Observatory, which is operated by the National Research Council of Canada. CHIME is funded by a grant from the Canada Foundation for Innovation (CFI) 2012 Leading Edge Fund (Project 31170) and by contributions from the provinces of British Columbia, Quebec, and Ontario. The CHIME/FRB Project is funded by a grant from the CFI 2015 Innovation Fund (Project 33213) and by contributions from the provinces of British Columbia and Quebec, and by the Dunlap Institute for Astronomy and Astrophysics at the University of Toronto. Additional support was provided by the Canadian Institute for Advanced Research (CIFAR), McGill University, and the McGill Space Institute thanks to the Trottier Family Foundation and the University of British Columbia. The CHIME/FRB baseband system is funded in part by a Canada Foundation for Innovation John R. Evans Leaders Fund award to I.H.S.

The Dunlap Institute is funded through an endowment established by the David Dunlap family and the University of Toronto.

Based on observations obtained at the Gemini Observatory, which is operated by the Association of Universities for Research in Astronomy, Inc., under a cooperative agreement with the NSF on behalf of the Gemini partnership: the National Science Foundation (United States), the Science and Technology Facilities Council (United Kingdom), the National Research Council (Canada), CONICYT (Chile), the Australian Research Council (Australia), Ministério da Ciência e Tecnologia (Brazil), and SECYT (Argentina). We appreciate the Gemini team for granting us observing time for the program ID: GN-2022B-Q-308.

B.M.G. acknowledges the support of the Natural Sciences and Engineering Research Council of Canada (NSERC) through grant RGPIN-2022-03163, and of the Canada Research Chairs program. M.R.D. acknowledges support from the NSERC through grant RGPIN-2019-06186, the Canada Research Chairs Program, the Canadian Institute for Advanced Research (CIFAR), and the Dunlap Institute at the University of Toronto. V.M.K. holds the Lorne Trottier Chair in Astrophysics & Cosmology, a Distinguished James McGill Professorship, and receives support from an NSERC Discovery grant (RGPIN-228738-13), and from the FRQNT CRAQ. K.W. M. holds the Adam J. Burgasser Chair in Astrophysics and is supported by an NSF Grant (2008031). A.B.P. is a Banting Fellow, McGill Space Institute (MSI) Fellow, and a Fonds de Recherche du Quebec—Nature et Technologies (FRQNT) postdoctoral fellow. Z.P. and P. S. are Dunlap Fellows. FRB Research at UBC is funded by an NSERC Discovery Grant and by the Canadian Institute for Advanced Research. The CHIME/FRB baseband system is funded in part by a CFI John R. Evans Leaders Fund award to I.H.S. M.B. is a Mcwilliams fellow. F.A.D is supported by the University of British Columbia (UBC) Four Year Fellowship. A.M.C is funded by an NSERC Doctoral Postgraduate Scholarship. K.S. is supported by the NSF Graduate Research Fellowship Program.

Facilities: CHIME, Gemini North.

Softwares: FRUITBAT (Batten 2019), PATH (Aggarwal et al. 2021), PYRAF (Science Software Branch at STScI 2012), Prospector (Johnson et al. 2021), emcee (Foreman-Mackey et al. 2013), python-fsps (Conroy et al. 2009), Astropy (Astropy Collaboration et al. 2018), Matplotlib (Hunter 2007), NumPy (Harris et al. 2020), SAOImage DS9 (Joye & Mandel 2003).

Appendix
PATH Probabilities of All Candidates

Here, we present the tables (Tables A1, A2, and A3) of probabilities of all the sources in the field of FRB 20200223B, FRB 20190110C, and FRB 20191106C. R_{50} is the half-light radius of the galaxy from the DESI survey, $P_{0.0}$ is the probability that the object is the preferred host galaxy of the FRB given the prior $P(U) = 0.0$, and $P_{0.1}$ is the probability that the object is the preferred host galaxy of the FRB given the prior $P(U) = 0.1$.

Table A1
PATH Probability for the Sources in the Field of FRB 20200223B

Source	R.A. (deg)	Decl. (deg)	R_{50} (arcsec)	r Band (mag)	$P_{0.0}$	$P_{0.1}$
1	8.269527	28.831267	5.814174	16.080395	0.994104	0.899497
2	8.266982	28.829577	0.405767	22.06333	0.001767	0.001599
3	8.267366	28.82594	0.646236	21.993284	0.001427	0.001291
4	8.263246	28.828137	0.434656	23.971949	0.000322	0.000291
5	8.263912	28.828986	0.877458	23.089138	0.000708	0.00064
6	8.268353	28.826364	0.439845	22.411278	0.000992	0.000897
7	8.271681	28.835329	0.450015	22.615425	0.000682	0.000617

Table A2
PATH Probability for the Sources in the Field of FRB 20190110C

Source	R.A. (deg)	Decl. (deg)	R_{50} (arcsec)	r Band (mag)	$P_{0.0}$	$P_{0.1}$
1	249.318485	41.443412	3.379357	18.00912	0.917943	0.779452
2	249.324262	41.442808	0.662556	22.32065	0.013446	0.011418
3	249.336069	41.448172	0.39331	21.21785	0.025025	0.02125
4	249.315487	41.448435	0.337111	23.374989	0.003773	0.003204
5	249.317587	41.444105	2.032882	21.900526	0.016519	0.014027
6	249.319692	41.437475	1.434205	23.942047	0.002159	0.001833
7	249.319796	41.440578	0.571469	22.459723	0.009711	0.008246
8	249.32092	41.448989	0.321152	23.473305	0.004379	0.003719
9	249.325318	41.441917	0.459996	23.032875	0.007045	0.005982

Table A3
PATH Probability for the Sources in the Field of FRB 20191106C

Source	RA (deg)	DEC (deg)	R_{50} (arcsec)	r Band (mag)	$P_{0.0}$	$P_{0.1}$
1	199.580129	42.999713	1.601871	17.306004	0.951259	0.815378
2	199.567778	43.005932	0.361793	23.50386	0.001473	0.001262
3	199.568633	43.007172	1.032621	21.765076	0.006658	0.005707
4	199.571617	42.998974	0.700418	22.764788	0.00331	0.002837
5	199.57512	42.99899	0.467756	22.17816	0.006046	0.005182
6	199.575607	43.007772	0.982723	21.274609	0.012805	0.010976
7	199.577994	43.000793	1.937793	23.018389	0.003076	0.002636
8	199.578285	42.994688	0.400479	23.901838	0.001067	0.000915
9	199.580623	43.009469	1.088066	22.449223	0.003727	0.003195
10	199.582184	42.998333	2.298028	21.562593	0.009444	0.008095
11	199.584588	43.000609	0.749572	23.984762	0.001136	0.000973

ORCID iDs

Adaeze L. Ibik https://orcid.org/0000-0003-2405-2967
Maria R. Drout https://orcid.org/0000-0001-7081-0082
B. M. Gaensler https://orcid.org/0000-0002-3382-9558
Paul Scholz https://orcid.org/0000-0002-7374-7119
Daniele Michilli https://orcid.org/0000-0002-2551-7554
Mohit Bhardwaj https://orcid.org/0000-0002-3615-3514
Victoria M. Kaspi https://orcid.org/0000-0001-9345-0307
Ziggy Pleunis https://orcid.org/0000-0002-4795-697X
Tomas Cassanelli https://orcid.org/0000-0003-2047-5276
Amanda M. Cook https://orcid.org/0000-0001-6422-8125
Fengqiu A. Dong https://orcid.org/0000-0003-4098-5222
Jane F. Kaczmarek https://orcid.org/0000-0003-4810-7803
Calvin Leung https://orcid.org/0000-0002-4209-7408
Kiyoshi W. Masui https://orcid.org/0000-0002-4279-6946
Aaron B. Pearlman https://orcid.org/0000-0002-8912-0732
Masoud Rafiei-Ravandi https://orcid.org/0000-0001-7694-6650
Ketan R Sand https://orcid.org/0000-0003-3154-3676
Kaitlyn Shin https://orcid.org/0000-0002-6823-2073
Kendrick M. Smith https://orcid.org/0000-0002-2088-3125
Ingrid H. Stairs https://orcid.org/0000-0001-9784-8670

References

Aggarwal, K., Budavári, T., Deller, A. T., et al. 2021, ApJ, 911, 95
Ahumada, R., Prieto, C. A., Almeida, A., et al. 2020, ApJS, 249, 3
Aihara, H., Allende Prieto, C., An, D., et al. 2011, ApJS, 193, 29
Alam, S., Albareti, F. D., Allende Prieto, C., et al. 2015, ApJS, 219, 12
Anderson, L. D., Bania, T. M., Balser, D. S., et al. 2014, ApJS, 212, 1
Astropy Collaboration, Price-Whelan, A. M., Sipőcz, B. M., et al. 2018, AJ, 156, 123
Avedisova, V. S. 2002, ARep, 46, 193
Baldwin, J. A., Phillips, M. M., & Terlevich, R. 1981, PASP, 93, 5

Banerjee, P., Szabo, T., Pierpaoli, E., et al. 2018, NewA, 58, 61
Batten, A. 2019, JOSS, 4, 1399
Becker, R. H., White, R. L., & Helfand, D. J. 1995, ApJ, 450, 559
Beloborodov, A. M. 2017, ApJL, 843, L26
Bhandari, S., Gordon, A. C., Scott, D. R., et al. 2023, ApJ, 948, 67
Bhandari, S., Heintz, K. E., Aggarwal, K., et al. 2022a, AJ, 163, 69
Bhandari, S., Heintz, K. E., Aggarwal, K., et al. 2022b, AJ, 163, 69
Bhandari, S., Sadler, E. M., Prochaska, J. X., et al. 2020, ApJL, 895, L37
Bhardwaj, M., Gaensler, B. M., Kaspi, V. M., et al. 2021a, ApJL, 910, L18
Bhardwaj, M., Kirichenko, A. Y., Michilli, D., et al. 2021b, ApJL, 919, L24
Bianchi, L., Shiao, B., & Thilker, D. 2017, ApJS, 230, 24
Bochenek, C. D., Ravi, V., Belov, K. V., et al. 2020, Natur, 587, 59
Cardelli, J. A., Clayton, G. C., & Mathis, J. S. 1989, ApJ, 345, 245
Carnall, A. C., Leja, J., Johnson, B. D., et al. 2019, ApJ, 873, 44
Cassanelli, T., Leung, C., Rahman, M., et al. 2022, AJ, 163, 65
Chabrier, G. 2003, PASP, 115, 763
Chang, Y.-Y., van der Wel, A., da Cunha, E., & Rix, H.-W. 2015, ApJS, 219, 8
Chatterjee, S., Law, C. J., Wharton, R. S., et al. 2017, Natur, 541, 58
CHIME/FRB Collaboration, Amiri, M., Andersen, B. C., et al. 2021, ApJS, 257, 59
CHIME/FRB Collaboration, Amiri, M., Bandura, K., et al. 2018, ApJ, 863, 48
CHIME/FRB Collaboration, Amiri, M., Bandura, K., et al. 2019a, Natur, 566, 235
CHIME/FRB Collaboration, Amiri, M., Bandura, K., et al. 2019b, ApJL, 885, L24
CHIME/FRB Collaboration, Andersen, B. C., Bandura, K., et al. 2023, ApJ, 947, 83
CHIME/FRB Collaboration, Andersen, B. C., Bandura, K. M., et al. 2020, Natur, 587, 54
Condon, J. J., Cotton, W. D., Greisen, E. W., et al. 1998, AJ, 115, 1693
Connor, L., Miller, M. C., & Gardenier, D. W. 2020, MNRAS, 497, 3076
Conroy, C., Gunn, J. E., & White, M. 2009, ApJ, 699, 486
Cook, A. M., Bhardwaj, M., Gaensler, B. M., et al. 2023, ApJ, 946, 58
Cordes, J. M., & Lazio, T. J. W. 2002, arXiv:astro-ph/0207156
Cui, X.-Q., Zhao, Y.-H., Chu, Y.-Q., et al. 2012, RAA, 12, 1197
Cutri, R. M., Skrutskie, M. F., van Dyk, S., et al. 2003, yCat, II/246
Dálya, G., Galgóczi, G., Dobos, L., et al. 2018, MNRAS, 479, 2374
Dey, A., Schlegel, D. J., Lang, D., et al. 2019, AJ, 157, 168
Dolag, K., Gaensler, B. M., Beck, A. M., & Beck, M. C. 2015, MNRAS, 451, 4277
Driessen, L. N., Barr, E., Buckley, D., et al. 2024, MNRAS, 527, 3659
Driver, S. P., Wright, A. H., Andrews, S. K., et al. 2016, MNRAS, 455, 3911
Eftekhari, T., & Berger, E. 2017, ApJ, 849, 162
Eftekhari, T., Berger, E., Margalit, B., et al. 2019, ApJL, 876, L10
Eftekhari, T., Margalit, B., Omand, C. M. B., et al. 2021, ApJ, 912, 21
Eisenstein, D. J., Weinberg, D. H., Agol, E., et al. 2011, AJ, 142, 72
Ellison, S. L., Teimoorinia, H., Rosario, D. J., & Mendel, J. T. 2016, MNRAS, 455, 370
Fong, W.-f., Dong, Y., Leja, J., et al. 2021, ApJL, 919, L23
Fonseca, E., Andersen, B. C., Bhardwaj, M., et al. 2020, ApJL, 891, L6
Foreman-Mackey, D., Hogg, D. W., Lang, D., & Goodman, J. 2013, PASP, 125, 306
Gordon, A. C., Fong, W.-f., Kilpatrick, C. D., et al. 2023, ApJ, 954, 80
Green, D. 2019, JApA, 40, 36
Gupta, P. D., & Saini, N. 2018, JApA, 39, 14
Harris, C. R., Millman, K. J., van der Walt, S. J., et al. 2020, Natur, 585, 357
Heintz, K. E., Prochaska, J. X., Simha, S., et al. 2020, ApJ, 903, 152
Hirschauer, A. S., Salzer, J. J., Janowiecki, S., & Wegner, G. A. 2018, AJ, 155, 82
Hunter, J. D. 2007, CSE, 9, 90
Intema, H. T., Jagannathan, P., Mooley, K. P., & Frail, D. A. 2017, A&A, 598, A78
Jankowski, F., Bezuidenhout, M. C., Caleb, M., et al. 2023, MNRAS, 524, 4275
Jarrett, T. H., Cluver, M. E., Magoulas, C., et al. 2017, ApJ, 836, 182
Johnson, B. D., Leja, J., Conroy, C., & Speagle, J. S. 2021, ApJS, 254, 22
Joye, W. A., & Mandel, E. 2003, in ASP Conf. Ser. 295, Astronomical Data Analysis Software and Systems XII, ed. X. I. I. Systems (San Francisco, CA: ASP), 489
Katz, J. I. 2017, MNRAS Lett., 471, L92
Kauffmann, G., Heckman, T. M., Tremonti, C., et al. 2003, MNRAS, 346, 1055
Kennicutt, R. C., Jr. 1998, ARA&A, 36, 189
Kewley, L. J., Dopita, M. A., Sutherland, R. S., Heisler, C. A., & Trevena, J. 2001, ApJ, 556, 121
Kewley, L. J., & Ellison, S. L. 2008, ApJ, 681, 1183
Kirsten, F., Marcote, B., Nimmo, K., et al. 2022, Natur, 602, 585
Komatsu, E., Dunkley, J., Nolta, M. R., et al. 2009, ApJS, 180, 330
Kuminski, E., & Shamir, L. 2016, ApJS, 223, 20
Lacy, M., Baum, S. A., Chandler, C. J., et al. 2020, PASP, 132, 035001
Laigle, C., McCracken, H. J., Ilbert, O., et al. 2016, ApJS, 224, 24
Lanman, A. E., Andersen, B. C., Chawla, P., et al. 2022, ApJ, 927, 59
Law, C. J., Bower, G. C., Burke-Spolaor, S., et al. 2018, ApJS, 236, 8
Law, C. J., Connor, L., & Aggarwal, K. 2022, ApJ, 927, 55
Lee, K., Khrykin, I. S., Simha, S., et al. 2023, ApJL, 954, L7
Leja, J., Speagle, J. S., Johnson, B. D., et al. 2020, ApJ, 893, 111
Leung, C., MenaParra, J., Masui, K., et al. 2021, AJ, 161, 81
Lorimer, D. R., Bailes, M., McLaughlin, M. A., Narkevic, D. J., & Crawford, F. 2007, Sci, 318, 777
Lunnan, R., Chornock, R., Berger, E., et al. 2014, ApJ, 787, 138
Machalski, J., & Condon, J. J. 1999, ApJS, 123, 41
Macquart, J.-P., Prochaska, J. X., McQuinn, M., et al. 2020, Natur, 581, 391
Mahony, E. K., Ekers, R. D., Macquart, J.-P., et al. 2018, ApJL, 867, L10
Mannings, A. G., Fong, W.-f., Simha, S., et al. 2021, ApJ, 917, 75
Marcote, B., Nimmo, K., Hessels, J. W. T., et al. 2020, Natur, 577, 190
McConnachie, A. W. 2012, AJ, 144, 4
Mckinven, R. & CHIME/FRB Collaboration 2022, ATel, 15679, 1
Mena-Parra, J., Leung, C., Cary, S., et al. 2022, AJ, 163, 48
Metzger, B. D., Margalit, B., & Sironi, L. 2019, MNRAS, 485, 4091
Michilli, D., Bhardwaj, M., Brar, C., et al. 2023, ApJ, 950, 134
Michilli, D., Masui, K. W., Mckinven, R., et al. 2021, ApJ, 910, 147
Moustakas, J., Coil, A. L., Aird, J., et al. 2013, ApJ, 767, 50
Nikutta, R., Hunt-Walker, N., Nenkova, M., Ivezić, Ž., & Elitzur, M. 2014, MNRAS, 442, 3361
Nimmo, K., & Chatterjee, S. 2023, Fast Radio Burst Community Newsl., 4
Nimmo, K., Chatterjee, S., & Petroff, E. 2023, Fast Radio Burst Community Newsl., 4
Nimmo, K., Hewitt, D. M., Hessels, J. W. T., et al. 2022, ApJL, 927, L3
Niu, C. H., Aggarwal, K., Li, D., et al. 2022, Natur, 606, 873
Padovani, P., Mainieri, V., Tozzi, P., et al. 2009, ApJ, 694, 235
Pettini, M., & Pagel, B. E. J. 2004, MNRAS Lett., 348, L59
Planck Collaboration, Aghanim, N., Akrami, Y., et al. 2020, A&A, 641, A6
Platts, E., Weltman, A., Walters, A., et al. 2019, PhR, 821, 1
Pleunis, Z., Good, D. C., Kaspi, V. M., et al. 2021, ApJ, 923, 1
Rajwade, K. M., Bezuidenhout, M. C., Caleb, M., et al. 2022, MNRAS, 514, 1961
Ravi, V., Catha, M., Chen, G., et al. 2023, ApJL, 949, L3
Rice, T. S., Goodman, A. A., Bergin, E. A., Beaumont, C., & Dame, T. M. 2016, ApJ, 822, 52
Schlegel, D. J., Finkbeiner, D. P., & Davis, M. 1998, ApJ, 500, 525
Scholz, P., Bogdanov, S., Hessels, J. W. T., et al. 2017, ApJ, 846, 80
Science Software Branch at STScI, 2012 PyRAF: Python alternative for IRAF, Astrophysics Source Code Library, ascl:1207.011
Sharma, K., Somalwar, J., Law, C., et al. 2023, ApJ, 950, 175
Shimwell, T. W., Hardcastle, M. J., Tasse, C., et al. 2022, A&A, 659, A1
Simard, L., Mendel, J. T., Patton, D. R., Ellison, S. L., & McConnachie, A. W. 2011, ApJS, 196, 11
Spitzer Science Center (SSC), Infrared Science Archive (IRSA) 2021, yCat, II/368
Tacchella, S., Conroy, C., Faber, S. M., et al. 2022, ApJ, 926, 134
Tremonti, C. A., Heckman, T. M., Kauffmann, G., et al. 2004, ApJ, 613, 898
Trouille, L., Barger, A. J., & Tremonti, C. 2011, ApJ, 742, 46
Vega, O., Clemens, M. S., Bressan, A., et al. 2008, A&A, 484, 631
Vieyro, F. L., Romero, G. E., Bosch-Ramon, V., Marcote, B., & del Valle, M. V. 2017, A&A, 602, A64
Wen, Z. L., & Han, J. L. 2015, ApJ, 807, 178
Wen, Z. L., Han, J. L., & Liu, F. S. 2009, ApJS, 183, 197
Wen, Z. L., Han, J. L., & Liu, F. S. 2012, ApJS, 199, 34
Wen, Z. L., Han, J. L., & Yang, F. 2018, MNRAS, 475, 343
Wright, E. L., Eisenhardt, P. R. M., Mainzer, A. K., et al. 2010, AJ, 140, 1868
Yamasaki, S., & Totani, T. 2020, ApJ, 888, 105
Zhang, B. 2018, ApJL, 867, L21